Functional Characterization of Potential New Agents for Cancer Immunotherapy

Functional Characterization of Potential New Agents for Cancer Immunotherapy

Xiaoxu Wang

A Thesis Submitted to the Faculty of

The Harvard Medical School

in Partial Fulfillment of the Requirements

for the Degree of Master of Medical Sciences in Immunology

Harvard University

Boston, Massachusetts.

May, 2018

Thesis Advisor: Dr. Gordon Freeman Xiaoxu Wang

Functional Characterization of Potential New Agents for Cancer Immunotherapy

Abstract

PD-1/PD-L1 checkpoint blockade has demonstrated promise in a variety of malignancies. The blockade of T cell inhibitory molecules PD-1 and PD-L1 can rejuvenate T cells and improve tumor cell killing. However, the overall response rate of PD-1/PD-L1 immunotherapy is only about 20-30%. One promising method to improve cancer immunotherapy is combinatory immunotherapies that target new receptors/ligands regulating T cell activity, so the functional characterization of these new receptors/ligands is urgent. Due to the functional importance of the B7 superfamily in T cell activation, I studied T cell regulating functions of two poorly characterized B7 superfamily members, IgC domain-truncated CD86 and butyrophilin-like 2 (BTNL2). To study their function in a natural cell-cell interaction scenario, the murine IgC domain-truncated CD86 or murine BTNL2 was cloned and transfected into Chinese Hamster Ovary Cells that already expressed MHC Class II IA^d. After co-culturing the transfectants, OVA peptide 323-339 and transgenic T cells from DO11.10 mice, I tested T cell proliferation and cytokine expression. The data suggested cell-membrane bound BTNL2 will moderately stimulate T cells and increase IFN-γ secretion significantly. Similarly, stimulatory results were also demonstrated with mBTNL2 hIgG1 fusion protein and recombinant mBTNL2 protein. The stimulatory effect of BTNL2 on T cell activation suggested that BTNL2 could be targeted as a T cell activity modulator or be a potential checkpoint ligand to be lentiviral delivered to dendritic cells as a therapy. My study indicated additional B7 proteins may be another potential target for combinatory cancer immunotherapy with PD-1/PD-L1 blockade.

Table of Contents

1. Chapter 1: Background 1

1.1. Checkpoint Blockade.....1

1.2 ICB Response and Resistance Mechanisms.....2

1.3 New Co-stimulatory Molecules, BTNL2 and Modified CD86.....6

2. Chapter 2: Materials and Methods.....11

2.1. Pre-activation of T cells.....11

2.2. T cell Proliferation with CHO Cells.....12

2.3. T cell Proliferation with Plate-Bound-Antibody.....12

2.4. Cytokine Analysis.....13

2.5. Truncation Design of CD86-IgV.....13

2.6. Primer Design, Gene In-fusion and Vector Insertion.....13

2.7. Gene Cloning.....14

2.8. Cell Transfection.....15

2.9. Transient Transfection.....15

2.10. Cell Sorting and Subcloning.....15

2.11. Flow Cytometry.....16

3. Chapter 3: Results 18

3.1. mBTNL2 Expression and Subclone Selection.....18

3.2. T cell Stimulation with CHO Cells.....19

3.3. T Cell Stimulation with Plate-Bound-Antibody.....24

3.4. Initial Generation of mCD86 Constructs without the IgC Domain.....26

3.5. Generation and Detection of Modified mCD86 without IgC.....28

4. Chapter 4: Discussion.....32

4.1. Limitation and Perspectives.....32

4.2. Perspective for Cancer Immunotherapy.....36

5. Bibliography 38

Figures

Figure 1. Hypothesis for different biological activity of IgC truncated CD86: Ability to engage cell surface CD28 but not CTLA4. In cell-cell interactions, the full length CD86, which has both IgC and IgV domain, could reach both CD28 and CTLA4. However, the IgC truncated CD86 could only reach CD28 but not CTLA4 and then results in a stronger T cell stimulation.

Figure 2. Cell sorting of initial transfected population and phenotyping of mBTNL2 subclones. (A) Cell sorting of CHO-IAd+mBTNL2 cells. Double staining of mouse-IAd and mBTNL2. (B) Three mBTNL2 subclones had the indicated expression.

Figure 3. T cell proliferation in the presence of mBTNL2. (A) Time schedule of naïve $CD4^+$ T cell proliferation assay (B) Naive $CD4^+$ T cell proliferation on day 2 and (C) Day 3.

Figure 4. Naive $CD4^+$ T cell cytokine expression analysis by Luminex. Naïve $CD4^+$ T cell cytokine expression analysis when OVA was 1μg/mL on (A) Day 2 or (B) Day 3.

Figure 5. T cell proliferation in the presence of mBTNL2. (A) Time schedule of pre-activated $CD4^+$ T cell proliferation assay (B) Naive $CD4^+$ T cell proliferation on day 2

Figure 6. Pre-activated $CD4^+$ T cell cytokine expression analysis on Day 2 by Luminex. Pre-activated $CD4^+$ T cell cytokine expression analysis when OVA was 1μg/mL.

Figure 7. Naïve $CD4^+$ T cell proliferation when co-cultured with soluble mBTNL2 hIgG1 fusion protein. Naïve $CD4^+$ T cells were co-cultured with mBTNL2-hIgG1, 1.25μg/mL anti-CD3 and 2.5 μg/mL anti-CD28 antibody. T cell proliferation was analyzed on (A) Day 2 and (B) Day 3, separately

Figure 8. Naïve $CD4^+$ T cell proliferation when co-cultured with soluble recombinant mBTNL2. Naïve $CD4^+$ T cell were co-cultured with rmBTNL2-His, 1.25μg/mL anti-CD3 and 5 μg/mL anti-CD28 antibody. T cell proliferation was analyzed on Day 2

Figure 9. Design of "mCD86 1st ATG, IgV+Stalk+TM+Cyto" construct. The primer "mCD86 IgV reverse" was compared with "mCD86 stalk+TM+Cyto, Forward". The highlighted sequence was the 15-bp overlap for fusion.

Figure 10. Schematic diagram of generating IgC domain truncated CD86. (A) Process of truncating IgC domain. (B) Structures of natural CD86 and modified CD86 generated in this project.

Figure 11. Expression of IgC truncated mCD86. (A) Double staining of mouse-IA^d and IgC truncated mCD86. (B) Expression detection of IgC truncated mCD86 or full-length m CD86 with three commercial conjugated antibodies from different clones and mCD28 or mCTLA4 fusion protein

Tables

Table 1. Primers for mCD86 cloning

Table 2. Constructs of IgC truncated mCD86

Acknowledgements

I would like to give my huge and sincere thanks to my thesis advisor Dr. Gordon Freeman of the Dana-Farber Cancer Institute. Dr. Freeman is so supportive that he always teaches me experimental techniques with patience by himself. He teaches me backgrounds and knowledge of each experiment. He guides me to create ideas and design experiment to approach our thoughts. He never leaves me alone when I have troubles upon my work and gave me a lot of confidence over the past year. Without Dr. Freeman, I can't accomplish my masters thesis. I'm so honored and lucky to be in Freeman Lab.

I would also like to thank to Dr. Kathleen Mahoney for giving me suggestions on my projects and thesis. I would also like to acknowledge Dr. Xia Bu, Dr. Maria C. Speranza, Dr. Ping Hua, Dr. Ye Gan and Dr. Baogong Zhu for being so generous and kind to help and teach me during my study, including mice tumor injection, tumor measurements, flow cytometry and molecular cloning.

Last but not the least, I would like to thank the MMSc program at HMS. Thanks to Dr. Shiv Pillai and Dr. Mike Carroll for their dedication to our program and guidance in my education. Thanks to Dr. Diane Lam for her teaching and Selina Sarmiento for her help during my masters study.

This work was conducted with support from Students in the Master of Medical Sciences in Immunology program of Harvard Medical School. The content is solely the responsibility of the authors and does not necessarily represent the official views of Harvard University and its affiliated academic health care centers.

1. Chapter 1: Background

1.1. Checkpoint Blockade

The immune system is essential for tumor eradication. However, the functions of the immune system tend to be suppressed in the tumor microenvironment (TME) by inhibitory immune checkpoint ligands and receptors. The two most well-known checkpoint receptors are cytotoxic T lymphocyte antigen 4 (CTLA4; also known as CD152) and programmed cell death protein 1 (PD-1; also known as CD279). Both the CTLA4 and PD-1 pathways can be blocked by antibody and then unleash T cell activation. The identification of ligands and pathways of these two major checkpoint ligands/receptors has led to a breakthrough in cancer treatment.

CTLA-4 is a CD28 homolog that is expressed on activated T cells and constitutively expressed on regulatory T cells (Treg). In naive T cells, CTLA4 can also be expressed but is kept intracellularly[1]. Similar to CD28, CTLA4 can also bind to B7 superfamily[2]. In both *in vitro* and *in vivo* environment, CTLA4 competes with CD28 for B7 binding to suppress immune activation and this is one mechanism of tumor escape from immune surveillance[3]. After the function of CTLA4 was identified as inhibitory to T cells [4], the antitumor efficiacy of CTLA4 blockade has been clearly established in metastatic melanoma [5]. Similarly, the PD-1: PD-Ligand pathway is another T cell inhibitory axis. PD-1 is expressed on activated B cells, dendritic cells (DCs), monocytes, activated T cells but not naive T cells. PD-1 is transiently expressed during the maturation from $CD4^{-}CD8^{-}$ double negative T cells to naive T cells in the thymus[6]. Since PD-L1[7] and PD-L2 (B7-DC)[8] [9], the ligands of PD-1 were identified, there have been various studies suggesting either stimulatory or inhibitory functions of PD-1[7, 8, 10]. The functional differences in PD-1 might be caused by engagement of different ligands, however, the most recognized function of PD-1 is its inhibitory role in T cell regulation. Other studies have explored downstream signaling of PD-1.

PD-1 can recruit SHP2 phosphatase, which dephosphorylates the CD3ζ ITAM sites of T cell receptors (TCR) and sites on CD28, thereby attenuating TCR/CD28 signaling and impeding T cell activation[11, 12].

Due to the efficacy of CTLA-4 and PD-1 antibody blockade in tumor therapy, the US Food and Drug Administration (FDA) has approved several PD-1 (Nivolumab and Pembrolizumab), PD-L1 (Atezolizumab, Durvalumab and Avelumab), and CTLA-4 (Ipilimumab) antibodies in various cancer types. However, the response efficacy is not universal in histologically different cancers and many patients are resistant to immune checkpoint blockade (ICB) or develop resistance gradually.

1.2. ICB Response and Resistance Mechanisms

The mechanisms mediating ICB resistance have been studied intensely. In general, for tumor extrinsic mechanisms, there are four distinct factors that contribute to resistance to ICB: tumor microenvironment, metabolic factors, environmental factors and other host related factors[13]. All these factors mediate resistance to ICB mainly by dampening T cell function or intervening in T cell vitality.

In the tumor microenvironment, T cells are under the control of immune suppressive metabolites, infiltrating immune cells and receptors. For example, depletion of the essential amino acid tryptophan by the activity of Indoleamine 2,3-dioxygenase (IDO) leads to T cell anergy and cell death by catalyzing the formation of immunosuppressive metabolite kynurenine. Kynurenine then suppresses T cell function and contributes to the low abundance of infiltrating lymphocytes within the TME[14]. Other immune suppressive cells and alternative immune checkpoint molecules that emerge in TME also inhibit ICB-initiated T cell functions. Treg cells, Th2 cells, and myeloid-

derived suppressor cells (MDSCs)[15, 16, 17] have been found in the tumor microenvironment to suppress immune cells, mostly T cells. Patients who responded to PD-1 blockade can acquire adaptive resistance to the therapy by upregulation of other immune suppressive checkpoints receptors, such as T-cell immunoglobulin mucin-3 (TIM-3)[18]. Besides immune suppressive cells and other alternative checkpoints, myelomonocytic cells as well as the stromal cells (e.g. cancer-associated fibroblasts) can also impair response to ICB by trapping T cells in stroma, extracellular matrix or inducing hypoxic conditions and IFN-dependent inhibitory pathways to reduce T cells in TME[16].

Metabolic condition is another factor restricting ICB efficacy. Efficient anti-tumor T cell function also relies on sufficient nutrition supply. The metabolic competition, especially glucose competition between tumor cells and T cells restricts T cells in a harsh living condition[19]. So, this might be responsible for some immune non-responsive cases where ICB cannot stimulate T cells if T cells lack the conditions for healthy proliferation.

Environmental factors (e.g. vitamins and microbiota) also effect the likelihood of ICB resistance. In a small patient poulation, vitamin E supplementation has been demonstrated to increase $CD4^+$: $CD8^+$ T cell ratio and increase T helper 1 cytokines interleukin 2 and IFN-γ production, which enhanceed T cell proliferation and functions in patients with advanced colorectal cancer[20]. Although whether combining vitamin E supplementation with ICB potentiates immunotherapy has yet to be determined, this study proposed a new potential combinatory immunotherapy of ICB and Vitamin E supplementation for advanced tumor treatment in future clinical trials. Another significant environmental factor influencing ICB resistance is microbiota. Microbiota have been known to shape lymphoid structure, epithelial function and T cell subsets[21]. Recently, several studies suggested the important roles that microbiota play in ICB. Q-PCR

analysis and microbiota reconstitution in germ free or broad-spectrum antibiotic treated mice showed that *B. thetaiotaomicron* and *B. fragilis* can promote CTLA-4 blockade's anti-tumor efficacy in mouse sarcoma by initiating IL-12-dependent Th1 immune responses[22]. Similar to CTLA-4 blockade, *Akkermansia muciniphila* also restored PD-1 blockade efficacy by recruiting $CCR9^{+}CXCR3^{+}CD4^{+}$ T cells into mouse TME in an IL-12-dependent manner[23]. These two independent experiments indicated the microbiota-induced IL-12 pathway is essential for both CTLA-4 and PD-1/PD-L1 blockade, though the causitive microbiota is different in these two experiments. Besides IL-12 pathway, 16S ribosomal RNA sequencing demonstrated that *Bifidobacterium* augmention of host dendritic cells is another factor for efficient ICB responses, which enables T cell priming and facilitates PD-L1 response[24]. All these studies suggested gut microbiome composition can affect the response of some tumors to ICB.

Individual background such as age, HLA type and distinct germline polymorphisms in immune cell receptors might also influences ICB resistance, although thorough studies are still in progress.

In addition to tumor extrinsic mechanisms, evolution of cancer cells also contributes to ICB resistance. The tumor intrinsic mechanisms include absence of antigens (e.g. low mutational burden, antigen mutation, antigen silencing or deletion, and alternative splicing), absence of antigen presentation (e.g. deletion in TAP, silenced HLA), genetic T cell exclusion (e.g. PD-L1 expression to exhaust T cells) and insensitivity to T cells (e.g. IFN-γ signaling pathway mutation or activating alternative pathways)[25, 26, 27].

The distinct ICB resistance mechanisms indicates that combinatorial immunotherapy inducing anti-tumor T cells and targeting different resistance pathways is a promising strategy for cancer treatment. For instance, the sequential immunotherapy of CTLA-4 blockade and irradiated

tumor cells engineered to secrete GM-CSF (GVAX) showed inflammation-mediated tumor rejection in metastatic melanoma and advanced ovarian carcinoma[28]. Since the T cells rejuvenated by ICB are pre-existing T cells, the presence of anti-tumor T cells before ICB is critical. Thus, another idea of combinatorial immunotherapy is inducing or adoptively transferring anti-tumor T cells and then enhancing T cell proliferation by ICB[29]. Chimeric antigen receptor T cells (CAR-T) therapy have been demonstrated to be enhanced by subsequent PD-1 blockade[30, 31].

Another combinatorial strategy is targeting different receptors/ ligands involved in T cell regulation. This strategy is based on the mechanistic studies and the fact that T cell exhaustion and activation are integrated consequences of T cell intracellular and extracellular signaling. For example, besides PD-1, there are other inhibitory receptors, including CTLA4, LAG3, TIM3, BTLA, CD160, 2B4 and TIGIT expressed on exhausted T cells that might be involved in T cell regulation by non-redundant pathways[32, 33]. Since CTLA-4 and PD-1 contribute to T cell anergy through different mechanisms with CTLA-4 competing with CD28 for B7 ligation, but PD-1 through T cell intracellular suppression, it is rational to combine CTLA-4 and PD-1/PD-L1 blockade. In agreement with this, the combination of ipilimumab (anti-CTLA4 antibody) and nivolumab (anti-PD-1 antibody) led to a quicker and greater tumor regression compared to monotherapy in advanced melanoma[34]. This intensified therapeutic effect has also been demonstrated in the phase I trial in the same patient population[35]. Other examples of combinations currently under investigation include LAG-3, Tim-3, and 4-1BB. LAG-3 (CD223) is a cell surface receptor expressed on activated T cells, B cells, NK cells that limits both $CD4^+$ and $CD8^+$ T cells proliferation[36]. Blockade of two inhibitory molecules, LAG3 and PD-1 synergistically improved the clearance of transplantable tumors[37]. Tim-3 is also a new inhibitory immune checkpoint receptor controlling Th1 and $CD8^+$ T cytotoxic T cell function. Targeting Tim-3 and PD-1

pathways at the same time showed a better anti-tumor response than blocking a single pathway[38]. All these studies suggest the prospect of targeting distinct inhibitory pathways in different cancers. An alternate method of reversing T cell anergy is providing a T cell stimulatory signal plus inhibiting suppressive signals. 4-1BB (CD137; TNFRS9) is an activation-induced costimulatory molecule that can activate cytotoxic T cells and increase IFN-γ secretion[39]. Combination of anti-4-1BB mAbs and anti-CTLA-4 mAbs induced complete tumor rejection in almost all mice without inducing autoimmunity, whereas, the monotherapy of either anti-4-1BB or anti-CTLA-4 mAbs alone only led to limited tumor regression in MC38 colon adenocarcinoma[40]. This idea has also been demonstrated in the combination of anti-CTLA-4 mAb with anti-glucocorticoid-induced tumor necrosis factor receptor family related gene (GITR) mAb[41]. Such promising results from combining immunotherapies emphasize the importance of discovery of new agents involved in the regulation of immune responses.

1.3. New Co-stimulatory Molecules, BTNL2 and Modified CD86

Optimal T cell activation needs at least two distinct signals: the non-self antigen signal or signal 1 presented by the major histocompatibility complex (MHC) class I or II and the costimulatory signal or signal 2 delivered by antigen presenting cells (APC)[42]. The absence of the costimulatory signal will cause T cell functional inactivation, called anergy. Recently, since the co-stimulatory signal is a key pathway regulating T cell function, researchers have focused on T cell /immune response regulation by manipulating the costimulatory pathway in a cancer scenerio[43]. What's more, the co-stimulatory pathway is essential in cancer immunotherapy because recent study has suggested the co-stimulatory CD28 pathway rather than the TCR signal pathway is the primary target of PD-1 recruited SHP2 phosphatase[12]. Since CTLA-4 also works through

interruption of the co-stimulatory pathway[3], we might be able to target new agents to overcome immune checkpoint induced inhibition by releasing the suppression or enhancing the co-stimulatory pathway. So, the costimulatory molecules, B7 superfamily members and B7 homologues are strong candidates as cancer immunotherapy targets. In my thesis, I started the functional characterization of one B7 homologue, butyrophilin-like 2 (BTNL2) and a new version of CD86 that only contains the IgV domain in the extracellular region (CD86 IgV-TM-Cyto). The long-term goal of this study is to contribute to the discovery of new agents for combinatorial cancer immunotherapy.

The conventional costimulatory pathway refers to the ligation of B7 superfamily member on antigen presenting cells and CD28 on T cells. Initially, there were only two B7 members, CD80 (B7-1) and CD86 (B7-2) within the superfamily, but latter genetic studies and homology analysis discovered more B7 superfamily members and B7 homologues. B7 superfamily now includes CD80 (B7-1), CD86 (B7-2), PD-L1 (B7-H1, CD274), PD-L2 (B7-DC, CD273), ICOS-Ligand (B7-H2, CD275), B7-H3 (CD276), B7-H4 (VTCN1), VISTA (B7-H5), B7-H6, and HHLA2 (B7-H7) [44, 45]. The two most famous B7 molecules, CD86 and CD80 both have an extracellular IgV and IgC domain. They share similar costimulatory function in both $CD4^+$ and $CD8^+$ T cell stimulation, B cells, macrophages and DCs[46, 47]. However, CD86 was usually emphasized compared to CD80 because CD86 is constitutively expressed on naive B cells, which indicates that CD86 is more important than CD80 in the initiation of immune responses[48]. The CD86 knockout mice also manifested a more severe immunodeficiency compared to CD80 knockout mice[49]. Moreover, CD80 forms back to back homodimers, but CD86 functions as a monomer[50, 51]. The monomeric state of CD86 also facilitates its *in vitro* study because it will be more accurate to use fusion protein to mimic the function of CD86. In fact, there was a fusion protein study showing

that human CD86 IgV domain fused with human IgG1-Fc (CD86 IgV-hIgG1) could lead to stronger T cell proliferation and cytokine expression than the natural CD86 that contains both IgV and IgC domains. More interestingly, the CD86 IgV-hIgG1 increased IFNγ, IL-4 and GM-CSF secretion moderately[52]. Compared to a superagonist anti-CD28 monoclonal antibody, which was criticized for causing a strong cytokine storm[53], CD86IgV induced less cytokines expression making CD86 IgV delivery potentially a less toxic cancer immunotherapy.

However, delivery of fusion protein CD86 IgV-hIgG1 is not the best way to target the costimulatory pathway. Similar to the CTLA-4 and PD-1/PD-L1 Ig fusion protein/antibody studies, the working mechanisms as well as metabolic dynamics of fusion proteins *in vivo* are not fully understood. The presence of the Fc region in a fusion protein can mediate antibody-dependent cell-mediated cytotoxicity (ADCC) and complement-dependent cytotoxicity (CDC) by binding to FcγR and C1q, respectively. The half-life of the fusion protein is also decreased by host myeloid cells, such as tumor-associated macrophages that express FcγR, which leads to accrual of anti-PD-1 mAbs in macrophages[54]. So, a better way to utilize CD86 IgV could be as a cell membrane molecule delivered by a viral vector. This requires the functional study of cell-bound CD86 IgV that was investigated in my study. I hypothesize that the distances for CD86 to reach its receptors determine the function of CD86. The distance for CD86 IgV domain to reach CD28 and CTLA4 are different. Since the angle between CTLA4 IgV domains is larger than CD28's IgV domain[51, 55], it is possible that the IgC domain truncated CD86 can still reach CD28 but not CTLA4. Thus, the truncated CD86 then would provide a stronger stimulatory signal (Fig. 1). Since this hypothesis is also based on cell-cell interaction, I tried to generate a cell membrane bound truncated CD86 that theoretically can't reach CTLA4 but can reach CD28 and tested if it could provide a stronger stimulatory signal to T cells.

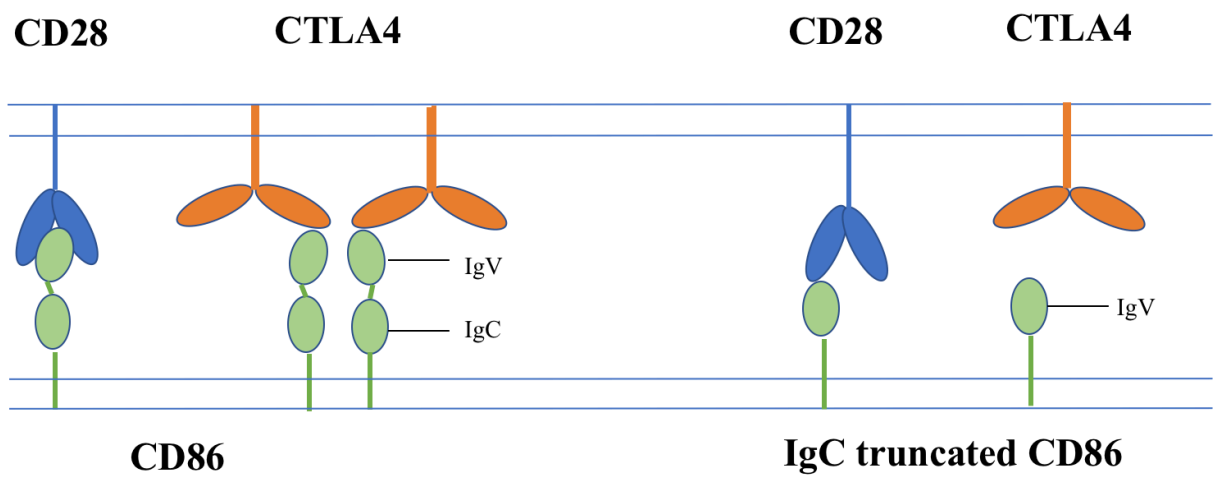

Figure 1. Hypothesis for different biological activity of IgC truncated CD86: Ability to engage cell surface CD28 but not CTLA4. In cell-cell interactions, the full length CD86, which has both IgC and IgV domain, could reach both CD28 and CTLA4. However, the IgC truncated CD86 could only reach CD28 but not CTLA4 and then results in a stronger T cell stimulation.

Besides the conventional costimulatory molecules, there is also a new B7 homologue subfamily involved in T cell co-stimulation, named the butyrophilin (BTN) family. BTN are cell surface proteins that belong to the Ig superfamily. BTN are in a gene cluster shared by human and mice. Many are located within the MHC locus, which contains a large number of genes related to immune responses[56]. In addition, BTN share sequence and structural similarity with the extracellular domain of B7. Phylogenetic study also suggested B7 and BTN superfamily have a common ancestor and clarified BTN as a new subfamily belonging within the B7 superfamily[57]. All these facts reveal the important immune functions that BTN may have. In general, BTN superfamily members have IgV and/or IgC domains in the extracellular domain and most members contain an intracellular B30.2/SPRY domain, except BTNL2. At this time, 13 BTN members have been identified in human and 11 BTN members in mouse. 6 of 11 mouse BTN members have

human orthologs: BTN1, BTN2A2, BTNL2, BTNL9, ERMAP, and MOG[58]. These orthologous BTN members shared by human and mouse make them good candidates for translational research.

Previously, some research groups investigated BTNL2 function with murine BTNL2-hIgG fusion protein[59, 60]. Their studies showed that BTNL2 will inhibit T cell proliferation when co-cultured with T cells. However, in their experiments, T cells were only incubated with plate-bound anti-CD3, BTNL2-hIg fusion protein with or without anti-CD28 antibody. Since anti-CD3 antibody has been demonstrated to be sometimes out-competed by other proteins during the coating step[61], the decreased T cell proliferation may be caused by low anti-CD3 antibody binding rather than inhibition by BTNL2. So, it is critical to coat anti-CD3 antibody and other proteins simultaneously to ensure the density of coated anti-CD3 antibody in plates[61]. Another problem of studying BNTL2 function using Ig fusion protein is the lack of cell-cell interaction that exists in an *in vivo* environment. Thus, the method of BTNL2's functional study still needs to be improved.

Genetic studies have also shed light on the function of BTNL2. A SNP analysis demonstrated that BTNL2 polymorphic variant rs2076530 is correlated with sarcoidosis and autoimmune diseases, including multiple sclerosis, type 1 diabetes, rheumatoid arthritis, and systemic lupus erythematosus[62, 63]. This primary disease-associated variant rs2076530 has a G to A transition in the splicing site in exon 5, which causes a 4-bp loss in the cDNA. The 4-bp loss then causes a frameshift and leads to an alternative BTNL2 variant without the C-terminal IgC and transmembrane domain. The researchers tested for the presence of BTNL2 and demonstrated that without the transmembrane domain, BTNL2 will be trapped in the cytosol instead of on the cell surface. This leads to loss of its function. Since people with this the risk-associated allele are prone to have sarcoidosis, it is possible that the BTNL2 is an immune inhibitory molecule. However, without the transmembrane domain, it is also possible to form a secreted soluble BTNL2. Although

for some molecules, the soluble form and cell-bound form have similar functions (e.g. cell-bound CTLA4 and soluble CTLA4), other molecules might have totally opposite function when present in different form. An example is MHC class I chain related molecule (MIC). MIC is the ligand of the natural killer group 2D (NKG2D). NKG2D is a transmembrane protein mainly expressed on NK cells. When expressed on the cell surface, MIC binds to NKG2D and then leads to NK cell activation. However, binding with the soluble form of MIC renders NKG2D-expressing cells inactive. So, it is worthy to confirm the function of BTNL2 both in soluble and cell membrane-bound forms with appropriate methods.

2. Chapter 2: Materials and Methods

2.1. Pre-activation of T cells

The spleens of 6-week old DO11. 10 mice were extracted, mashed and suspended in MCAS buffer (PBS, pH 7.2, with 0.5% bovine serum albumin, and 2 mM EDTA). Splenocytes were then lysed by Red Blood Cell Lysing Buffer Hybri-Max™ (Sigma-Aldrich, MA, USA) for one time or until the cell pellets were white. Naive CD4+ T cells were purified from splenocytes with mouse CD4+ T Cell Isolation Kit from Miltenyi Biotec Inc. (Auburn, CA, USA) at this step. For pre-activated T cells, as reported in our previous study[9], the splenocytes without red blood cells were co-cultured with 1 μg/mL OVA 323-339 for 72hrs. After this pre-activation, CD4+ T cells were purified with the same CD4+ T Cell Isolation Kit from Miltenyi Biotec Inc. (Auburn, CA, USA). CD4+ T cells were rested overnight in T cell cultivation media before re-stimulation. The components of T cell cultivation media were as described before with a few modifications[9]: 500mL RPMI-1640 (Life Technologies, Grand Island, New York) supplemented with fetal bovine serum (10%, Sigma), L-glutamine (2 mM), penicillin (100 U/ml), streptomycin (100 μg/ml), HEPES (10 mM), 2-mercaptoethanol (50 μM), which were all from Life Technologies.

2.2. T cell Proliferation with CHO Cells.

After being counted, 100,000 $CD4^+$ naive T cells or pre-activated $CD4^+$ T cells were plated into 96-well flat bottom plates with 10,000 mitomycin-pretreated CHO- IA^d or CHO- IA^d+ mBTNL2 cells. These two cell lines were cultured with OVA 323-339 in different concentrations: 0, 0.001, 0.01, 0.1, and 1 μg/mL. Each concentration had three duplicates. After cultivation at 37 ℃, 5% CO_2 for 48 and/or 72 hrs (naive T cells were cultured 48 and 72 hrs. Pre-activated T cells were cultured only for 48hrs), 50μl supernatant was harvested from each well and frozen at -80℃ for cytokine analysis. Then, 100 μl T cell culture media with 1 μCi tritiated thymidine was added. After additional 24hrs cultivation, T cells were harvested onto Printed Filtermat A (PerkinElmer, MA, USA) by Tomtec Cell Harvester (Tomtec, Inc, Hamden, CT). The Filtermats were then dried at room temperature for 16 hrs or until the Filtermats dried completely. The amount of tritium in Filtermats was analyzed by 1450 MicroBeta TriLux (PerkinElmer, MA, USA).

2.3. T cell Proliferation with Plate-Bound-Antibody

1.25 μg/mL anti-CD3 antibody (Bio X Cell, Cat. # BE0001-1, clone 145-2C11), 2.5 or 5 μg/ml Anti-CD28 antibody (Bio X Cell, Cat. # BE0015-1, clone 37.51) with various concentrations (10 μg/ml, 5 μg/ml, 2.5 μg/ml, 1.25 μg/ml, 0 μg/ml) of mBTNL2-hIgG1 or recombinant mBTNL2 (rmBTNL2) from R&D (R&D Systems, Inc. Minneapolis, MN, USA) were diluted in PBS and coated onto the 96-well flat bottom plates at 4℃ overnight. CD4+ T cells were purified from TIM-1 or TIM-4 knockout mice spleens by negative selection with CD4+ T Cell Isolation Kit from Miltenyi Biotec Inc. (Auburn, CA, USA). Then, for each antibody-coated well, 100,000 purified $CD4^+$ T Cell were added. Similar to the "T cell proliferation with CHO cells"

section, T cells were incubated at 37 ℃, 5% CO_2 for 48 or 72 hrs. 50μl supernatant was saved for further analysis. T cells were incubated with tritiated thymidine as above and analyzed by Tomtec Cell Harvester.

2.4. Cytokine Analysis

The cytokine analysis was performed with Luminex high performance mouse assay kit (R&D Systems, Inc. Minneapolis, MN, USA) to test the secretion of CCL5/RANTES, IFN-gamma, IL-10, IL-2, IL-27, IL-4, IL-6, IL-17, GM-CSF, TNF-alpha.

2.5. Truncation Design of CD86-IgV

To clone murine CD86 IgV-TM-Cyto (mCD86 IgV-TM-Cyto), murine CD86 gene and protein sequences were downloaded from National Center for Biotechnology Information (NCBI) and UCSC Genome Browser. For the mCD86, the sequences of different domains were identified based on previous reports, protein database UniProt and exons that the domains resided in. mCD86 contains the signal peptide, IgV, IgC, small stalk between IgC and transmembrane domain (TM), TM and Cytoplasmic domain (Cyto) containing exons. After the identification of mCD86 domains, 2 pairs of primers were designed to amplify mCD86 except the IgC domain by Hot start polymerase chain reaction (Thermo Scientific, MA, USA). The mCD86 without IgC domains were then cloned in two pieces with 15 bp overlaps between the pieces: (1). Signal-IgV domain and (2). stalk+ TM+ Cyto. All the other alternative mCD86 gene constructs were obtained using the same procedures. All primers of mCD86 are listed in Table 1. The schematic diagram is shown in Figure 10.

2.6. Primer Design, Gene In-fusion and Vector insertion.

In-Fusion® HD Cloning Kit (Takara Bio, CA, USA) was used to join different pieces of mCD86 genes. All the procedures followed In-Fusion® HD Cloning Kit and technical supporting paper[64]. In general, any two pieces of DNA with a 15-bp overlap can be joined by the In-Fusion enzyme. All the forward primers designed for mCD86 IgV domain have a 15-bp overlap with both mCD86 and 5' open side of vectors for insertion. All the reverse primers for mCD86 IgV domain and forward primers for stalk+ TM+ Cyto domain share a 15-bp overlap in the joining part. Last, all the reverse primers for mCD86 stalk+ TM+ Cyto domain have a 15-bp overlap with the 3' open side of vector for insertion. Each forward primer for mCD86 DNA IgV domain contains a Kozak consensus start site (CCACCATG). One example for designing the primers is shown in Figure 9. In each In-Fusion reaction, 1:2 molar ratio of vector and each inserted piece of DNA was used to ensure high fusion efficiency. In-Fusion reactions were incubated in the PCR machine 30 min at 42℃, then hold at 4℃. Forty μl TE was added prior to storing the products or proceeding to bacteria transformation.

2.7. Gene Cloning

mCD86 domain specific gene pieces were amplified by hot start PCR. Then, the corresponding pieces were fused and inserted into pEF vectors containing puromycin or hygromycin B-resistance gene with In-Fusion® HD Cloning Kit. The DNA products were immediately transformed into One Shot™ TOP10 Chemically Competent *E. coli* (Thermo Scientific, MA, USA). After 16hrs incubation at 37℃, single colonies were cultured overnight for plasmid extraction and sequencing. All the sequences of mCD86 constructs were verified by sequencing.

2.8. Cell Transfection

After linearization, mCD86 IgV constructs were electroporated into Chinese hamster ovary cells expressing MHC Class II IA^d (CHO- IA^d+ mCD86 w/o IgC) and murine pre-B-cell line 300.19 (300.19+ mCD86 w/o IgC). The previous lab-generated linearized mBTNL2 vectors were co-electroporated into CHO-IA^d cells with pEF vectors containing puromycin-resistance gene. After 2 days' cultivation, the cells transfected with mCD86 IgV fragments were then selected in 1000 μg/mL hygromycin B or 5 μg/mL puromycin. The cells transfected with mBTNL2 fragments (CHO- IA^d+ mBTNL2) were also selected in 5 μg/mL puromycin after two day's cultivation. Cells were kept under selection until the cells were resistant to hygromycin B or puromycin.

2.9. Transient Transfection

3 x 10^6 HEK293T cells or COS cells were plated in a 100 mm tissue culture dish with 15ml D10 media the day before transfection. On the second day, cells were transfected using plasmid DNA and Genejuice (MilliporeSigma, Burlington, MA, USA). Briefly, for each 100 mm dish, transfected with 6 μg DNA dissolved in 600 μl Opti-MEM™ I Reduced Serum Media (Thermo Scientific, MA, USA) containing 18 μl Genejuice. The cells were harvested and analyzed by flow cytometry after 60 hrs cultivation at 37℃, 10% CO_2.

2.10. Cell Sorting and Subcloning

For cell sorting, 5 x 10^6 target cells were stained with 0.5 mL antibody at 10 μg/mL (diluted in sterile PBS with 2% FBS). The stable transfected CHO- IA^d+ mCD86 w/o IgC, 300.19+ mCD86 w/o IgC and CHO- IA^d+ mBTNL2 were stained with Alexa Fluor® 647-conjugated anti-mouse

IA^d (Clone 39-10-8, Biolegend, MA, USA), PE conjugated anti-mouse mCD86 (Clone GL-1, BD Bioscience, MA, USA) or PE conjugated anti-mouse BTNL2 antibody (clone 311.8A7) and then sorted by M Aria II SORP (BD Biosciences, MA, USA). Each cell line was sorted into bulk population in 15 ml tubes. After the sorted cells grew up, cells were stained for the second time with the same procedure but sorted into single cells in 96-well round plates for 300.19 cells and flat-bottom for CHO cells. Single cell clones were stained with the same anti-mCD86 or mBTNL2 antibodies used in cell sorting and analyzed by BD FACSCanto™ II (BD Biosciences, MA, USA). The most stable clones with the highest mBTNL2 or mCD86 expression were selected to grow up.

2.11. Flow Cytometry

Both the untransfected CHO- IA^d, tranfected CHO- IA^d cells, COS cells and HEK293T cells were harvested by PBS with 1mM EDTA. The cells expressing different mCD86 IgV constructs were stained with PE conjugated anti-mouse CD86 antibody from Biolegend Inc (Cat. # 105106, clone PO3), Invitrogen (Cat. # MA5-17953, clone RMMP-2), BD Bioscience (Cat. # 550542, clone GL-1), unconjugated anti-mouse CD86 antibody from R&D Systems (Lot. # UE0112011, polyclonal antibody), murine CTLA4-hIgG1, murine CD28-hIgG1 fusion protein (lab generated). The CHO- IA^d+ mBTNL2 were stained with lab generated PE conjugated anti-mBTNL2 antibody (clone 311. 8A7). For the unconjugated antibody, 50,000 cells (50 µl, 2.5 x 10^6 cells/ml) were stained with 50 µl antibody at 10 µg/mL in 96-well round bottom plates. After incubation at 4℃ for 30 mins, cells were washed with FACS buffer (PBS with 2% fetal bovine serum, 0.02% azide and additional 0.5mM EDTA if the cells were adherent cells) twice. The secondary antibodies (50 µl, 10 µg/mL) were added immediately after cells were washed twice. Similarly, cells were incubated at 4℃ for 30 mins. After two washes with FACS buffer, cells were

fixed with Fix buffer (PBS with 2% formaldehyde). For staining with fluorophore-conjugated antibodies, cells were fixed after washing the primary conjugated antibody twice with FACS buffer.

3. Chapter 3: Results

3.1. mBTNL2 Expression and Subclone Selection.

To better characterize mBTNL2 function in a cell-cell contact manner, mBTNL2 was co-transfected into CHO-IA^d cells with the pEF vector contained puromycin resistance gene. After 7 days selection under 5 μg/mL puromycin, mBTNL2 transfected CHO- IA^d cells were phenotyped with anti- mouse IA^d and anti-mBTNL2 antibodies (Fig. 2A). To get single cell clones with stable and high mBTNL2 expression, CHO- IA^d+mBTNL2 were then sorted into single cell. After the clones grew up, we picked up and phenotyped 10-15 biggest cell clones, which grew faster. Although all the sorted clones were IA^{d+} mBTNL2$^+$, the expression level of mBTNL2 was variable between clones. Three phenotyping results of single cell clones are shown in Fig 2B. They represented the three different expression patterns that single clones might have. In the Fig 2B, clone 1 was frozen for further experiments due to its high expression (high fluorescence) and stable (narrow peak) mBTNL2 expression.

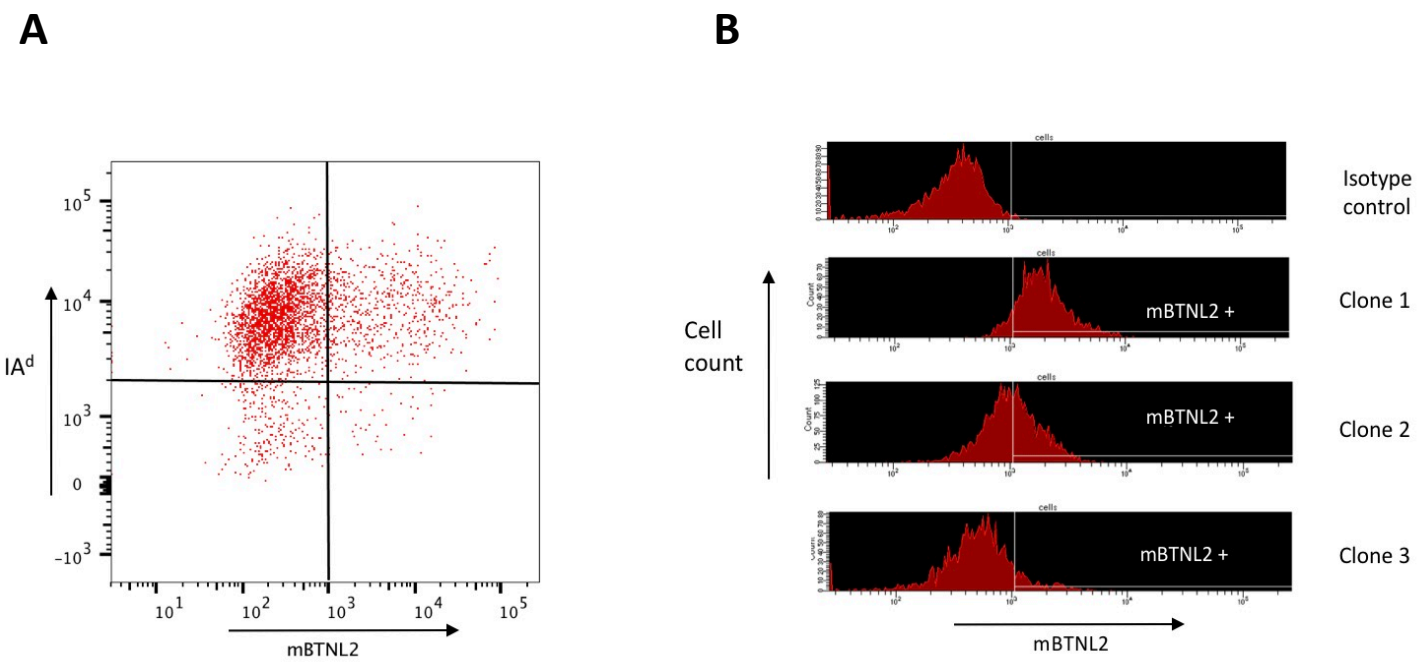

Figure 2. Cell sorting of initial transfected population and phenotyping of mBTNL2 subclones. (A) Cell sorting of CHO-IA^d+mBTNL2 cells. Double staining of mouse-IA^d and mBTNL2. (B) Three mBTNL2 subclones had the indicated expression.

3.2. T cell Stimulation with CHO Cells

To set an appropriate control for CHO- IA^d +mBTNL2 cells in the T cell proliferation assay, a CHO- IA^d cell clone that has similar IA^d expression level should be identified. So, when co-cultured with naive CD4$^+$ T cells, CHO- IA^d +mBTNL2 and CHO- IA^d could initiate the same extent of TCR signal. To get the suitable cell clone, the untransfected CHO- IA^d cells were subcloned by serial dilution in 96-well plates. The subclones with matched IA^d expression were selected by phenotyping and flow cytometry. All CHO- IA^d clones were re-phenotyped with CHO- IA^d +mBTNL2 in the same plate to avoid differences caused by plate differences. Based on staining results, CHO- IA^d, clone C10 was paired with CHO- IA^d +mBTNL2, clone F1. The CHO-

IA^d +mBTNL2, clone F1 or CHO- IA^d, clone C10 were co-cultured with $CD4^+$ T cells from DO11.10 mice in 96-well plates. DO11.10 were TCR transgenic mice with a TCRs that can recognize OVA 323-339 peptide presented by IA^d. The naive $CD4^+$ activation process is described in Figure 3A. CHO and $CD4^+$ T cells were co-cultured with OVA 323-339 at various concentrations. The Naive $CD4^+$ T cell proliferation analysis by tritiated thymidine incorporation on day 2 (after 48 hrs cultivation) showed that both the CHO- IA^d and CHO- IA^d +mBTNL2 groups initiate detectable T cell proliferation when the OVA peptide concentration was higher than 0.01μg/mL (Fig 3B, 3C). When OVA was 0.1μg/mL, T cell proliferation in CHO- IA^d +mBTNL2 group became significantly higher compared to CHO- IA^d group. However, when OVA concentration increased to 1μg/mL, the significance disappeared (Fig 3B). This non-significant result might be caused by high standard deviation on CHO- IA^d +mBTNL2 group, but it was clear that cell-membrane bound mBTNL2 provided a stimulatory signal to T cells. We also tested T cell proliferation on Day 3 (after 72 hrs cultivation). However, because of the accumulated T cell proliferation and relatively small amount of media contained in each 96-well, the T cells were overgrown in the poor nutrition environment and reached the maximum that they could proliferate in 96-well plates (Fig. 3C). Consistent with the visual and microscopic observation, tritiated thymidine incorporation analysis showed similar extent of proliferation in CHO- IA^d +mBTNL2 and CHO- IA^d group (Fig. 3C). To further confirm the T cell proliferation and understand downstream immune response after T cell activation, we tested the cytokine expression in this system by luminex. We analyzed CCL5/RANTES, IFN-gamma, IL-10, IL-2, IL-27, IL-4, IL-6, IL-17, GM-CSF, TNF-alpha expression after CD4+ T cells were cultured for 48 and 72 hrs. On Day 2 (48 hrs cultivation), the negative control group not containing antigen presenting cells or CHO cells had no cytokine expression (Fig. 4A). In two other experimental groups that had CHO-

IA^d +mBTNL2 or CHO- IA^d, most cytokines were undetectable. The three cytokines expressed most highly were GM-CSF, IL-2, and TNF-alpha, but all of them were at a very low concentration of around or less than 100pg/mL and there was no significant difference between CHO- IA^d +mBTNL2 and CHO- IA^d group (Fig. 4A). The presence of mBTNL2 did not significantly alter the induction of IL-2 expression, yet T cells grew faster in CHO- IA^d +mBTNL2 group. On day 3 (72 hrs cultivation), the CCL5/RANTES, IL-4 and IL-10 increased in the CHO- IA^d +mBTNL2 group compared to data on Day 2. On Day 3, a significant difference in the expression of IFN-γ was seen in the CHO- IA^d +mBTNL2 group, while the expression of CCL5/RANTES, IL-4 and IL-10 were not significantly different from CHO- IA^d group on Day 3 (Fig. 4B). This indicated that mBTNL2 might play some role in the initial T cell activation. Also, in spite of the significant difference in expression of IFN-γ, the total amount of cytokine expression was low. Since it takes time for cytokine genes to be transcribed and translated, T cells won't have lots of cytokine expression after their initial activation.

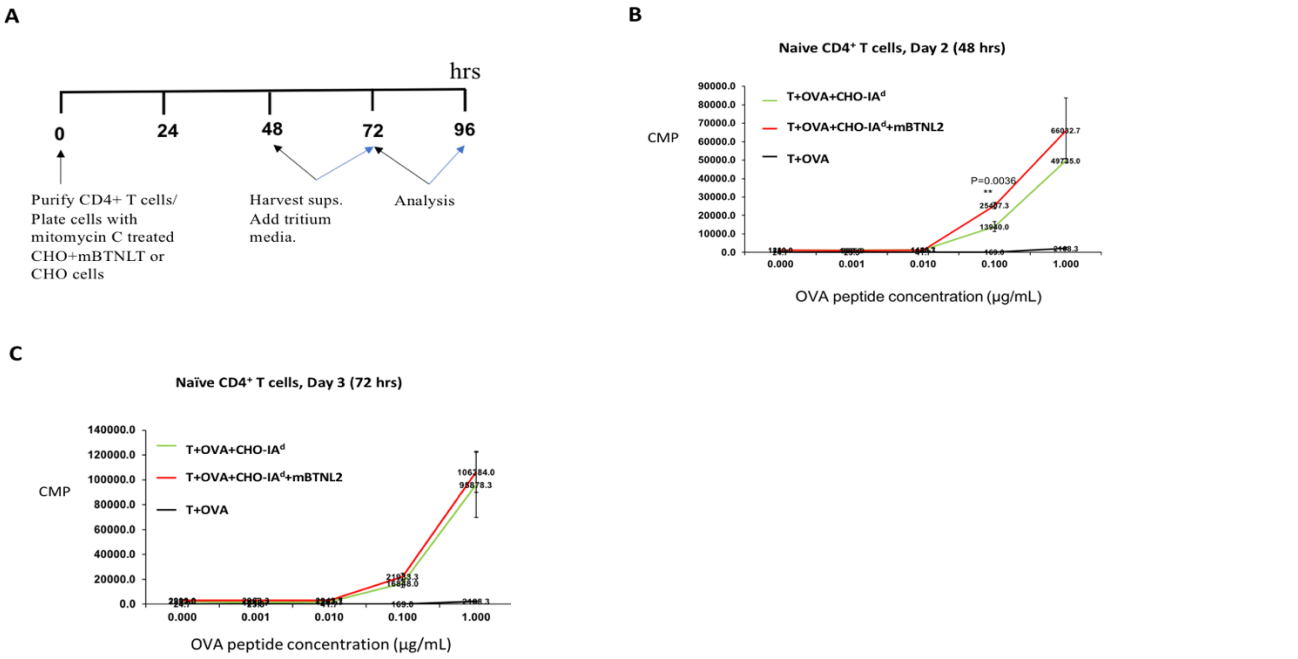

Figure 3. T cell proliferation in the presence of mBTNL2. (A) Time schedule of naïve $CD4^+$ T cell proliferation assay (B) Naive $CD4^+$ T cell proliferation on day 2 and (C) Day 3.

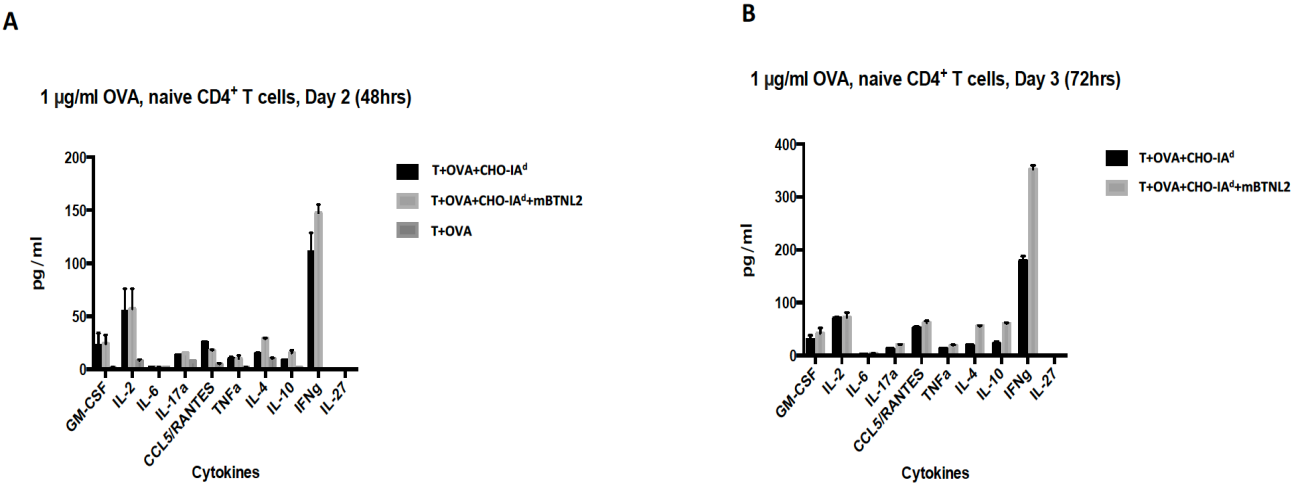

Figure 4. Naive $CD4^+$ T cell cytokine expression analysis by Luminex. Naïve $CD4^+$ T cell cytokine expression analysis when OVA was 1µg/mL on (A) Day 2 or (B) Day 3.

To solve this problem, we pre-activated T cells before adding them into 96-well plates and re-tested the T cell proliferation and cytokine expression. The T cell activation timelines was indicated in Fig. 5A. Briefly, the splenocytes including $CD4^+$ T cells from DO11.10 mice were pre-activated for 3 days (72hrs) in media containing 1 μg/mL OVA peptide. However, even only co-cultured with CHO cells for 2 days, pre-activated $CD4^+$ T cells were overgrown and similarly, there was no significant difference between mBTNL2 and untransfected CHO cell group (Fig. 5B). The pattern of cytokines expressed by pre-activated T cells changed compared to naive T cells (Fig 6). While IFN-γ again was one of the most expressed cytokines, GM-CSF and CCL5/RANTES were induced to a greater extent, and GM-CSF was significantly higher in the CHO- IA^d +mBTNL2 group (Fig. 6). CCL5/RANTES had been suggested to be involved in mast cell recruitment[65] and GM-CSF involved in recruitment of neutrophils, monocytes and lymphocytes[66]. These results indicate that mBTNL2 might direct T cell differentiation and contribute to myeloid cell recruitment.

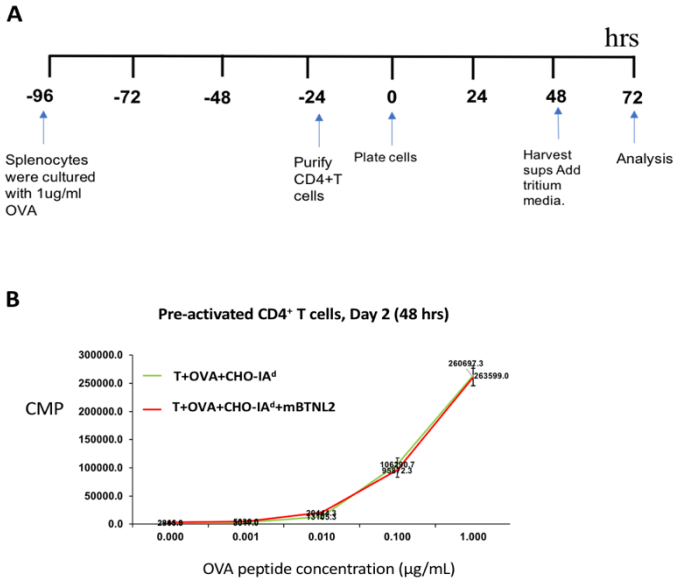

Figure 5. T cell proliferation in the presence of mBTNL2.
(A) Time schedule of pre-activated $CD4^+$ T cell proliferation assay (B) Naive $CD4^+$ T cell proliferation on day 2

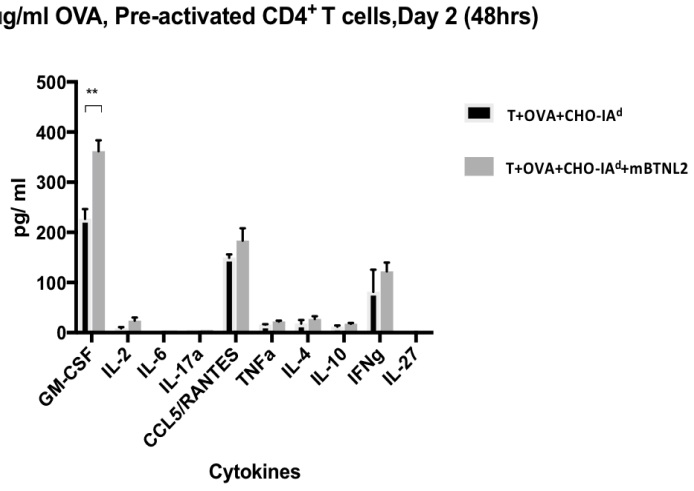

Figure 6. Pre-activated $CD4^+$ T cell cytokine expression analysis on Day 2 by Luminex. Pre-activated $CD4^+$ T cell cytokine expression analysis when OVA was 1µg/mL.

3.3. T Cell Stimulation with Plate-Bound-Antibody

As mentioned in Chapter one, soluble proteins sometimes have different functions than the cell-membrane bound version. Also, since T cell stimulation assays with plate-bound-antibody sometimes are not very accurate due to competition by other proteins for binding sites on the plastic plate, we repeated the T cell proliferation assay with plate-bound-antibody and different concentrations of recombinant mBTNL2 with a C-terminal 6-His tag (rmBTNL2-His) or mBTNL2-hIgG1 fusion protein. In this T cell proliferation system, because we wanted to test the function of the soluble form of mBTNL2, we couldn't use mBTNL2 transfected CHO cells to present OVA (Signal 1) and deliver signal 2. So, we used anti-CD3 and anti-CD28 antibodies to mimic signal 1 and 2 to T cells. The soluble mBTNL2s we used were the rmBTNL2 and mBTNL2-hIgG1 protein. The naive $CD4^+$ T cells were purified and cultured in 96-well plate for two days or three days before analysis. Since this *in vitro* system was in 96-well plates, to avoid over-proliferation of T cells, we only coated 1.25 µg/mL anti-CD3 and 2.5 or 5 µg/mL anti-CD28

antibodies, which we determined before was appropriate for 100,000 $CD4^+$ T proliferation for 2 or 3 days. The results demonstrated that on both Day 2 or Day 3, T cell proliferation always showed a mBTNL2-hIgG1 concentration dependent increase (Fig 7). Similar results were also observed in the rmBTNL2 group (Fig 8). So, in agreement with the cell-membrane-bound mBTNL2, soluble mBTNL2 also always provided a stimulatory signal to T cells.

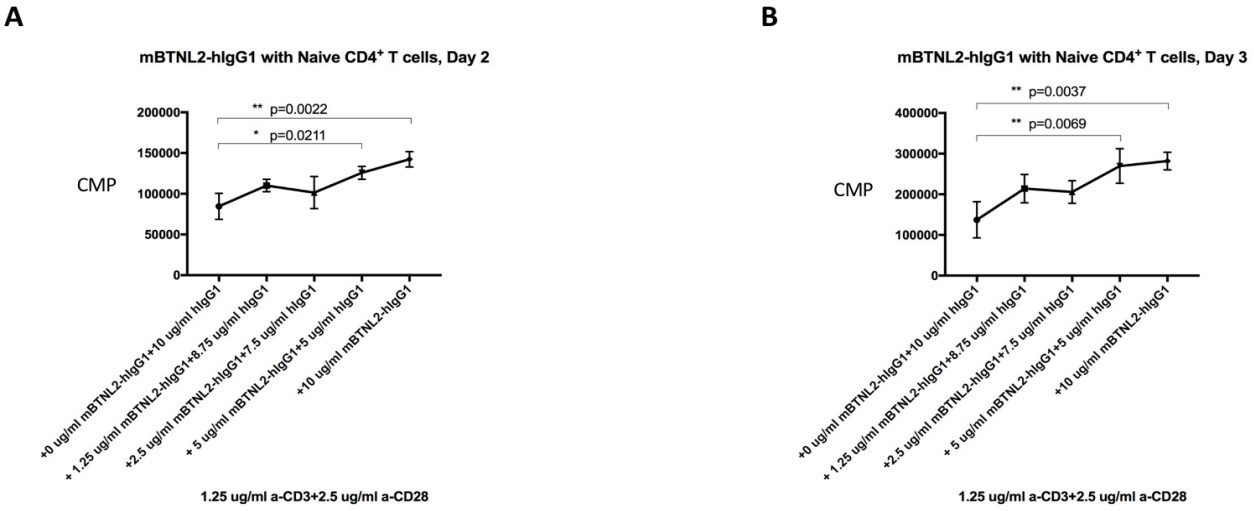

Figure 7. Naïve $CD4^+$ T cell proliferation when co-cultured with soluble mBTNL2 hIgG1 fusion protein. Naïve $CD4^+$ T cells were co-cultured with mBTNL2-hIgG1, 1.25μg/mL anti-CD3 and 2.5 μg/mL anti-CD28 antibody. T cell proliferation was analyzed on (A) Day 2 and (B) Day 3, separately

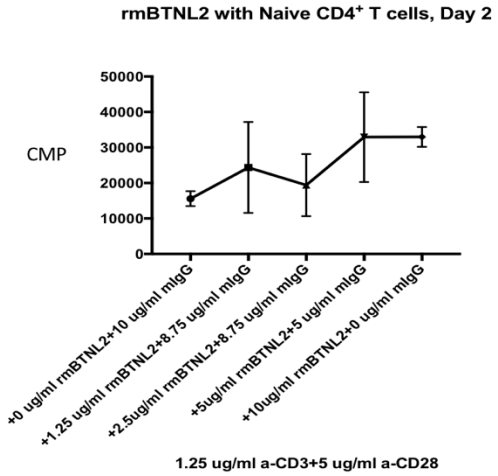

Figure 8. Naïve CD4$^+$ T cell proliferation when co-cultured with soluble recombinant mBTNL2. Naïve CD4$^+$ T cell were co-cultured with rmBTNL2-His, 1.25μg/mL anti-CD3 and 5 μg/mL anti-CD28 antibody. T cell proliferation was analyzed on Day 2

3.4. Initial Generation of mCD86 Constructs without the IgC Domain

mCD86 Signal-IgV domain and Stalk+TM+Cyto domains were cloned and fused to remove the IgC domain and form a new version of mCD86, mCD86 IgV-TM-Cyto (Fig. 9, 10). Since mCD86 has two ATGs at the beginning of the signal domain, two primers starting at each ATG were designed, called "mCD86 First ATG IgV, Forward" and "mCD86 second ATG IgV, Forward" (Table 1). The Signal-IgV domain of mCD86 was then cloned and fused with Stalk+TM+Cyto domain (Table 2, constructs 1 and 2). After insertion into pEF-puro vectors, these two constructs were then transfected into CHO-IA^d cells, separately.

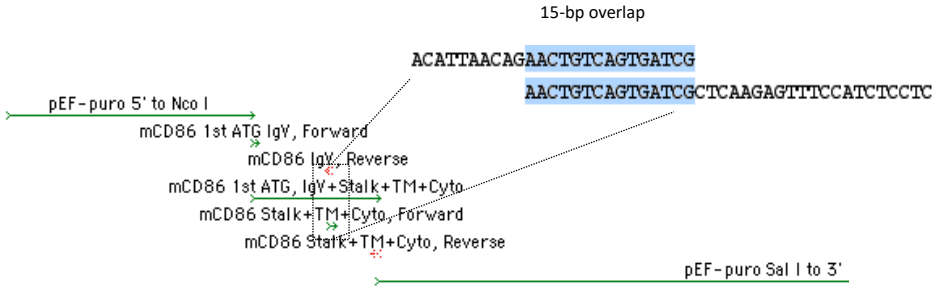

Figure 9. Design of "mCD86 1st ATG, IgV+Stalk+TM+Cyto" construct. The primer "mCD86 IgV reverse" was compared with "mCD86 stalk+TM+Cyto, Forward". The highlighted sequence was the 15-bp overlap for fusion.

The expression of mCD86 1st or 2nd IgV-TM-Cyto on cell surface was detected by flow cytometry. However, neither mCD86 1st ATG or 2nd

IgV-TM-Cyto could be detected by PE conjugated anti-mouse mCD86 (Clone GL-1) (Fig 11B). Previous studies suggested GL-1 anti-CD86 antibody could block $CD8^+$ T cell priming *in vivo* and *in vitro*[67]. The IgV domain of CD86 and CD80 contains the binding region for CD28 and CTLA-4. The IgC domain is not needed for CD28 or CTLA-4 binding. Since antibodies targeting the IgV domain can block T cell costimulation, the GL-1 antibody should be able to recognize mCD86 IgV-TM-Cyto in theory. To avoid the possibility that the epitope recognized by the GL-1 antibody was influenced by the absence of the IgC domain, additional anti-CD86 antibodies from different commercially available clones were tested: RMMP-2, PO-3 and polyclonal anti-CD86 antibodies. Since CD28 and CTLA4 are ligands of CD86[4], murine CTLA4-hIgG1 and murine CD28-hIgG1 fusion proteins were also used for detection of mCD86 by flow cytometry. Still, none of these antibodies or fusion proteins were able to detect mCD86 IgV-TM-Cyto on CHO-IA^d (Fig 11B). To avoid the possibility that the host cell, CHO-IA^d might not be suitable for mCD86 IgV-TM-Cyto expression, we electroporated mCD86 IgV-TM-

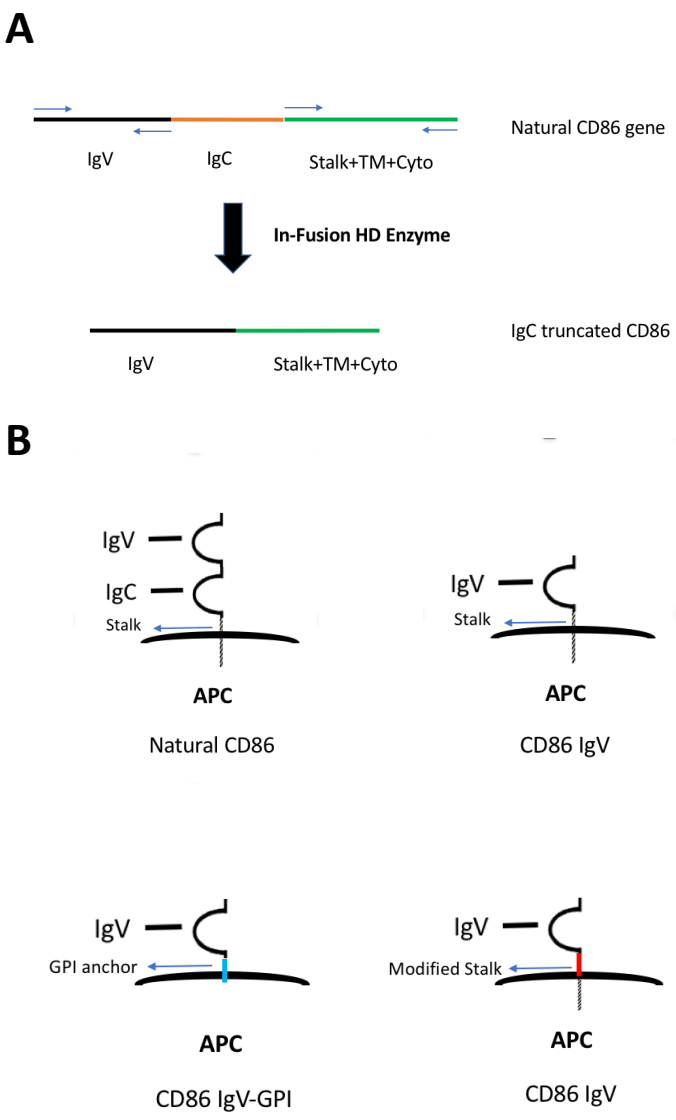

Figure 10. Schematic diagram of generating IgC domain truncated CD86. (A) Process of truncating IgC domain. (B) Structures of natural CD86 and modified CD86 generated in this project.

Cyto fragments into 300.19 cells, which is a murine pre-B-cell line that could express mCD86 theoretically. We also transfected 293T and COS cells by transient transfection, which ensures higher copy number of transfected gene and generally leads to high level protein expression. These three transfected cells were analyzed with all the anti-CD86 antibodies and fusion protein mentioned. Unfortunately, although the cells transfected with full length mCD86 could be detected to various extents, no mCD86 IgV-TM-Cyto expression was detected (Fig.11B). These results drove us to consider that the structure of mCD86 IgV-TM-Cyto might be too unstable to be expressed.

Oligos	Sequence 5' →3'
mCD86 First ATG IgV, Forward	TTCAAATCCACCATGGACCCCAGATGCACCATG
mCD86 second ATG IgV, Forward	TTCAAATCCACCATGGGCTTGGCAATCCTTATC
mCD86 IgV, Reverse	CGATCACTGACAGTTCTGTTAATGT
mCD86 Stalk+TM+Cyto, Forward	AACTGTCAGTGATCGCTCAAGAGTTTCCATCTCCTC
mCD86 Stalk+TM+Cyto, Reverse	AGTAACGTTAGTCGACCTCACTCTGCATTTGGTTTTGC
mCD86 Signal+IgV, GPI anchor, Reverse	GCTGCTTGGGCTTAAGATCACTGACAGTTCTGTTAATGT
mCD86 with 5' UTR at Hind III, Forward	GTGTCGTGAGAAGCTTGAACAACCAGACTCCTGTAGACGTGTTCC -AGAACTTACGGAAGCACCCACGATGGACCCCAGATGCACCATG
mCD86 IgV (Isoleucine Junction), Reverse	ACATTAACAGAACTGTCAGTGATC
mCD86 (follow Isoleucine) Stalk+TM+Cyto, Forward	GAACTGTCAGTGATCCAAGAGTTTCCATCTCCTCAAACG
mCD86 IgV (Isoleucine Junction), GG-GPI, Reverse	GCTGCTTGGGCTTAAGCCTCCGATCACTGACAGTTCTGTTAATGT
mCD86 IgV (Isoleucine Junction), GG+Stalk+TM+Cyto, Forward	GAACTGTCAGTGATCGGAGGCCAAGAGTTTCCATCTCCTCAAACG
mCD86 IgV (Isoleucine Junction), GPI, Reverse	ACATTAACAGAACTGTCAGTGATCTTAAGCCCAAGCAGC
mCD86 First ATG, IgV Glyco mutation N→D. Forward	TTCAAATCCACCATGGACCCCAGATGCACCATGGGCTTGGCAATCCTTATCTTTGTGACAGTC -TTGCTGATCTCAGATGCTGTTTCCGTGGAGACGCAAGCTTATTTCGATGGGACTGCATATCTG
mCD86 First ATG, IgV Glyco mutation T→A. Forward	TTCAAATCCACCATGGACCCCAGATGCACCATGGGCTTGGCAATCCTTATCTTTGTGACAGTC -TTGCTGATCTCAGATGCTGTTTCCGTGGAGACGCAAGCTTATTTCAATGGGGCTGCATATCTG

Table 1. Primers for mCD86 cloning

3.5. Generation and Detection of Modified mCD86 without IgC.

I proposed several hypotheses to explain why mCD86 IgV-TM-Cyto couldn't be expressed and we modified the structures of mCD86 IgV-TM-Cyto accordingly. First, I tested a GPI anchor to guide mCD86 expression onto the cell surface. Previous research demonstrated the introduction of GPI anchor led to expression of transfected gene on the apical surface of Madin-Darby Canine

Kidney Epithelial Cells[68]. Since T cells interact with CD86 through the IgV domain, it shouldn't cause functional changes by introducing a GPI anchor derived from a human CD58 cDNA. So, we designed the primers to clone the mCD86 IgV, ending with GPI anchor (Table 2, constructs 3, 4). The new mCD86 IgV constructs were inserted into pEF-Puro-GPI vector generated by Freeman lab. However, we tested the mCD86 IgV expression with all the 6 antibodies and fusion proteins, but no expression was seen.

Number	mCD86 Structure	Vector
1	mCD86 1st ATG, IgV+Stalk+TM+Cyto	pEF-Puro
2	mCD86 2nd ATG, IgV+Stalk+TM+Cyto	pEF-Puro
3	mCD86 1st ATG IgV, GPI anchor	pEF-Puro-GPI anchor
4	mCD86 2nd ATG IgV, GPI anchor	pEF-Puro-GPI anchor
5	mCD86 1st ATG, IgV (Isoleucine Junction)+GPI anchor	pEF-Puro-GPI anchor
6	mCD86 2nd ATG, IgV (Isoleucine Junction)+GPI anchor	pEF-Puro-GPI anchor
7	mCD86 1st ATG, IgV (Isoleucine Junction)+GG+GPI anchor	pEF-Puro-GPI anchor
8	mCD86 2nd ATG, IgV (Isoleucine Junction)+GG+GPI anchor	pEF-Puro-GPI anchor
9	mCD86, additional 5'UTR+IgV((Isoleucine Stalk)+TM+cyto	pEF-Puro
10	mCD86, additional 5'UTR+IgV+TM+cyto	pEF-Puro
11	mCD86 1st ATG, IgV (Isoleucine Junction)+Stalk+TM+Cyto	pEF-Puro
12	mCD86 2nd ATG, IgV (Isoleucine Junction)+Stalk+TM+Cyto	pEF-Puro
13	mCD86 1st ATG, IgV (Isoleucine Junction)+GG+Stalk+TM+Cyto	pEF-Puro
14	mCD86 1st ATG, IgV (Isoleucine Junction), Threonine→ Alanine+GG+Stalk+TM+Cyto	pEF-Hygro
15	mCD86 1st ATG, IgV (Isoleucine Junction), Asparagine→ Aspartic Acid+GG+Stalk+TM+Cyto	pEF-Hygro
16	mCD86 1st ATG, IgV (Isoleucine Junction), Threonine→ Alanine+GG+GPI anchor	pEF-Puro-GPI anchor
17	mCD86 1st ATG, IgV (Isoleucine Junction), Asparagine→ Aspartic Acid+GG+GPI anchor	pEF-Puro-GPI anchor
18	mCD86 1st ATG, IgV Threonine→ Alanine+Stalk+TM+Cyto	pEF-Hygro
19	mCD86 1st ATG IgV Asparagine→ Aspartic Acid+Stalk+TM+Cyto	pEF-Hygro
20	mCD86 1st ATG IgV +Stalk+TM+Cyto from GenScript	pcDNA3.1/Hygro(+)
21	mCD86 1st ATG IgV +Tim 1 mucin like domain from GenScript	pcDNA3.1/Hygro(+)

Table 2. Constructs of IgC truncated mCD86

For a second approach, I removed 3 nucleotides from the end of IgV domain (Table 2, constructs 5-9,11-17). According to the previous result, the human IgG fusion protein with human CD86 IgV ended after a leucine was successfully expressed and secreted[52]. So, we mimicked the condition of human CD86 IgV and removed 3 nucleotides from the end of IgV domain to make

mCD86 IgV end at isoleucine, which also has a hydrophobic side chain as does leucine. However, we were still unable to detect mCD86 IgV expression.

Then, we considered that the structure of the truncated mCD86 could make the fusion protein unstable. To reduce the steric hindrance between CD86 IgV domain and the membrane surface, we used multiple methods to increase IgV domain's distance to the cell membrane, including adding two additional glycines to increase the distance between membrane and IgV domain (Table 2, constructs 7,8, 13-17). The additional two glycines were added by primer design and In-Fusion technique. We also mutated the glycosylation site at the bottom of mCD86 IgV domain (Table2, constructs 14-19). Glycosylation, a process where glycans are attached to protein, lipids, or other organic molecules, will affect the volume occupied by the protein. Asn-Xaa-Ser/Thr has been demonstrated as the motif for N-linked glycosylation[69]. In the protein sequence of mCD86 IgV, there are two Asn-Xaa-Ser/Thr residing in position 33-35 (N-G-T) and position 47-49 (N-I-S). According to the crystal structure of mCD86, the glycosylation site at position 33-35 (N-G-T) is at the bottom of IgV domain. Since the IgV domain of mCD86 without IgC is much closer to the membrane than the IgV domain in full length CD86, the glycan attached to CD86 IgV might cause steric hindrance with the membrane surface. To avoid this hindrance, we mutated the asparagine at position 33 into Aspartic Acid or mutated Threonine at position 35 into Alanine. All these point mutations were introduced by primers. Unfortunately, these modifications didn't improve the truncated mCD86 expression. To further increase the distance from IgV domain to cell membrane, we finally fused mCD86 IgV with the long, extended Tim 1 mucin like domain and conducted codon optimization, which done by GenScript (NJ, USA) (Construct 21) and then tested expression of truncated mCD86. However, no matter which antibody or fusion protein was used, expression was not observed.

In yeast the 5' untranslated region (UTR) of mRNA can impact protein expression level [70]. To identify if the expression of modified mCD86 was impacted by 5' UTR, we added the CD86 natural 54-bp long 5' UTR sequence, starting from the Hind III restriction site to the beginning of signal peptide sequence (Constructs 9-10). The addition of the natural 5'UTR did not improve the expression of mCD86 by FACS analysis.

After testing multiple constructs for protein expression, we questioned whether the vectors and codon preference might also influence truncated mCD86 expression. So, the initial protein sequence of "mCD86 IgV, 1st ATG +Stalk+TM+Cyto" (Table 2, construct 1) was sent to GenScript (NJ, USA) to conduct codon optimization in CHO cell system. After codon optimization, the synthesized gene (Table 2, construct 20) was inserted into a different mammalian expression vector, pcDNA3.1/Hygro(+) which uses different promoters and polyadenylation sites. The optimized construct was transiently transfected into 293T or COS cells. The cell-surface protein expression was tested by flow cytometry with different anti-CD86 antibodies (clone PO3, RMMP-2, GL-1 and polyclonal antibody), CTLA4-hIgG1 and murine CD28-hIgG1 fusion protein. However, this construct also did not demonstrate mCD86 expression (Data Not Shown). In total, I made 21 constructs with various structures to express the truncated mCD86, but none produced detectable protein on the cell surface.

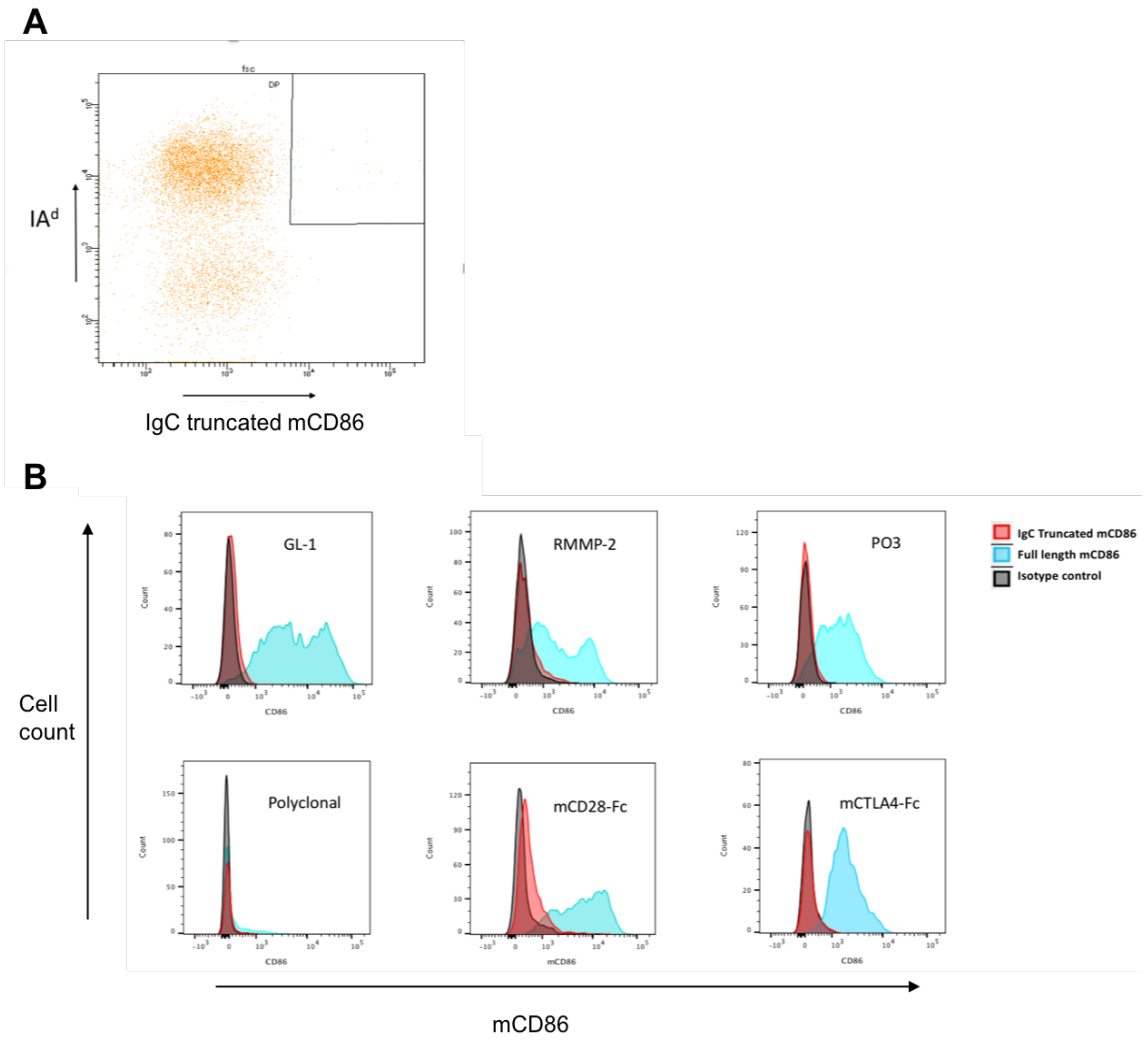

Figure 11. Expression of IgC truncated mCD86. (A) Double staining of mouse-IA^d and IgC truncated mCD86. (B) Expression detection of IgC truncated mCD86 or full-length m CD86 with three commercial conjugated antibodies from different clones and mCD28 or mCTLA4 fusion protein

4. Chapter 4: Discussion

4.1. Limitation and Perspectives

My work comprised the functional characterization of two co-stimulatory molecules: IgC-truncated mCD86 and mBTNL2. Although the projects with mBTNL2 progressed smoothly, the truncated mCD86 project was much more challenging. In the end, I made and tested 21 different

constructs of truncated mCD86, but none were successful. Even though I have discussed several different strategies to increase and validate the expression of truncated mCD86, there are still aspects we can improve for future projects. Despite this trouble shooting, we do not understand the reasons why truncated mCD86 expression can't be detected. Truncated mCD86, therefore, could be a special molecule for understanding mechanisms controlling truncated protein stability and expression.

In fact, a similar construct of CD80 is reported to be expressed. Since the IgC truncated human CD80 fusion protein could be generated[52], I expected that the corresponding mouse truncated CD86 should also easily be generated but such was not the case. The failure of any detectable expression of truncated mCD86 could be caused by several possibilities. First, the truncated mCD86 was not transcribed or translated. However, we didn't study which process is the limiting step. To address this question, it is possible to perform the western blot and RT-PCR to detect mCD86 protein and mRNA synthesis, separately. Second, mCD86 can be translated but failed to be translocated onto the cell surface. It has been reported that signal peptides can influence protein expression. In this case, we could in the future fuse mCD86 IgV domain with signal peptides derived from human albumin or human Kappa light chain[71] to enhance protein translocation. Third, the anti-CD86 antibodies and CTLA4 or CD28 fusion protein might not be suitable for truncated mCD86 detection due to protein folding. The epitopes of CD86 detected by these fusion proteins by antibodies or ligands might require the IgC domain, since one report says the IgC domain also contains epitopes essential for CD28 and CTLA4 binding[72] though the co-crystal structure shows contact only with the IgV domain. To solve this problem, a fluorescent tag, such as GFP, could be attached to the mCD86 protein. So, the expression can be detected by fluorescence microscopy or flow cytometry. This truncated mCD86 project also provide several

interesting questions for investigation. In many B7 superfamily members the IgC domain is conventionally considered less important than IgV domain. For example, based on our previous results, the expression and PD-1 binding capacity of IgC truncated PD-L1 would not be influenced by IgC truncation (paper has been accepted but not published yet). However, from my project, the IgC domain actually could be more important for CD86 than we expected. The IgC domain could affect quaternary structure, receptor binding and co-signaling function for CD80 and CD86 [73]. Interestingly, although the whole molecular structure and receptor binding structure of human CD86 has been well described, the murine CD86 structure is poorly understood as no crystal structure has been reported. If the crystal structure of mCD86 was analyzed, we will be able to better understand how mCD86 interacts with CTLA4, CD28 and the roles that the IgC domain plays in this process and determine whether it is conserved in human CD86. Understanding the function of the CD86 IgC domain may determine why this domain is vital for some B7 molecules, but not for others, and improve our ability to modulate specific immune costimulatory pathways.

If the IgC truncated CD86 can be expressed on the surface and the stronger stimulatory effects of IgC truncated CD86 can be confirmed in the future, as suggested by the reported fusion protein study[52], a lentivirus vector or oncolytic virus could be used for IgC truncated CD86 delivery to tumor cells or dendritic cells[74]. Checkpoint blockade is an immunotherapy based on proteins. However, the Fc region in antibodies complicates the antibody mechanisms in *in vivo* environments. Nowadays, since viral vectors have been designed to be less toxic and viral delivery could bypass the complex mechanisms of fusion protein, the IgC truncated CD86 and other stimulatory molecules could be delivered to tumor-bearing mice or patients in the future.

My second project about mBTNL2 suggested it has a stimulatory role in T cell activation. This result is opposite to the previous mBTNL2 study with fusion proteins. In immunology, it is

not uncommon that different research groups have demonstrated the opposite function for one molecule, such as PD-L1[7, 10] and B7-H3[75, 76, 77]. I have discussed the possible scenarios where a naturally stimulatory molecule reads out as inhibitory in previous sections. However, as PD-L1 (B7-H1) was initially described by some, inhibitory molecules might be described as stimulatory based on some in vitro assays. The discrepancy could be caused by the purity of recombinant proteins and antibodies, such as the presence of Lipopolysaccharides (LPS). LPS is a component of gram-negative bacteria that can be present in agents and its concentration is measured as Endotoxin Units (EU). In general, 10 EU/mg is the threshold for T cell activation. So, using reagents with EU above 10 EU/mg can give misleading T cell activation results. It is important to assay purified protein reagents for endotoxin level, filter all reagents and keep them in a sterile, low EU status. In the cytokine expression assay, although T cell proliferation and cytokine expression were testable in this *in vitro* system, the overgrowth of T cells became a major factor that contributed to inaccuracy. To reconfirm the stimulatory effect of mBTNL2, we could analyze T cell proliferation by CSFE, which would compare the T cell proliferation in a detailed manner. Also, my functional study about mBTNL2 is all *in vitro*. To further understand BTNL2 function and avoid misleading results, we could generate BTNL2 knockout mice, so we can observe the phenotypes and test immune responses in different tumor models. The cytokine expression analysis also demonstrated high GM-CSF and CCL5/RANTES expression in CHO-IA^d+mBTNL2 group. This suggested that BTNL2 was important for myeloid cell recruitment by regulating T cells. It will be worthwhile to test whether and how BTNL2 affects T cells signaling and differentiation, as well as myeloid cell in the tumor microenvironment in the future.

To create clinically useful fusion proteins and monoclonal antibodies as cancer immunotherapies, it will be critical to identify the ligands of BTNL2. Understanding the ligands

of BTNL2 and the molecular mechanisms of T cell regulation by BTNL2 could better characterize BTNL2 function and lay the foundation for BTNL2-based immunotherapy. The ligands of BTNL2 might be identified by protein microarray that screens the binding of BTNL2 with other proteins from a protein library.

4.2. Perspective for Cancer Immunotherapy

T cells can be unleashed with ICB. However, the working mechanism of ICB is complex. In spite of high response rate and durable benefit of PD-1 checkpoint blockade in Hodgkin's lymphoma, the majority tumor types are only moderately responsive to ICB. To increase the overall response rate, future studies should focus on the mechanistic study of ICB, including what is the detailed working mechanisms and the reasons contributing to ICB resistance.

Combinatorial immunotherapy will become more and more important for cancer treatment. The success of combining anti-CTLA4 and anti-PD-1 has led to FDA approval in metastatic melanoma and kidney cancer. Combinations such as anti-LAG3 and anti-PD-1 have achieved promising outcomes in early clinical trials. However, there are still some seemingly promising combinatorial immunotherapies that failed for unknown reasons. One example is the combination of anti-OX40 and anti-PD1. The agonist OX40 (anti-CD134 antibody) is a T cell activator when stimulated by its ligand. In theory, by enhancing T cell activation it should lead to stronger anti-tumor efficacy. However surprisingly, clinical study of anti-CD134 and anti-PD1 showed that this combination was actually detrimental because adding anti-PD-1 antibody in the initial period of anti-CD134 therapy led to T cell apoptosis compared to monotherapy with anti-PD1 [78]. This experience indicated that although the function and working mechanism of each individual immunotherapy may be fairly clear, the consequences and mechanisms of combinatorial

immunotherapy are not completely predictable. So, in the future, verifying the mechanisms of how combinations improve on the benefit of monotherapy with PD-1 blockade is critical. We should also generate a systematic methodology to measure the efficacy and safety of potential combinatorial immunotherapies before moving into clinical trials.

Another direction for cancer immunotherapy is the incorporation of artificial intelligence and neural networks. Cancer vaccines are another immunotherapy that could be combined with checkpoint blockade. However, the neoantigens for vaccines are hard to identify. Artificial intelligence and neural networks provide a new way for neoantigen discovery. In the past, studies have suggested that epitopes could be predicted by neural network[79]. So, a similar principle could also be applied to neoantigen prediction in cancer immunotherapy, such as neoantigen vaccine. In fact, some research institutes have formed the Tumor Neoantigen Selection Alliance last year. Although, neoantigen prediction still faces big challenges, including high cost and large workload in validating, neoantigen prediction is also a new trend for future personalized cancer immunotherapy.

5. Bibliography

1. Jago, C.B., Yates, J., Camara, N.O., Lechler, R.I. & Lombardi, G. Differential expression of CTLA-4 among T cell subsets. *Clin Exp Immunol* **136**, 463-471 (2004).

2. Linsley, P.S. *et al.* CTLA-4 is a second receptor for the B cell activation antigen B7. *J Exp Med* **174**, 561-569 (1991).

3. Ahmad, M., Rees, R.C. & Ali, S.A. Escape from immunotherapy: possible mechanisms that influence tumor regression/progression. *Cancer Immunol Immunother* **53**, 844-854 (2004).

4. Krummel, M.F. & Allison, J.P. CD28 and CTLA-4 have opposing effects on the response of T cells to stimulation. *J Exp Med* **182**, 459-465 (1995).

5. Lipson, E.J. & Drake, C.G. Ipilimumab: an anti-CTLA-4 antibody for metastatic melanoma. *Clin Cancer Res* **17**, 6958-6962 (2011).

6. Nishimura, H. *et al.* Developmentally regulated expression of the PD-1 protein on the surface of double-negative (CD4-CD8-) thymocytes. *Int Immunol* **8**, 773-780 (1996).

7. Freeman, G.J. *et al.* Engagement of the PD-1 immunoinhibitory receptor by a novel B7 family member leads to negative regulation of lymphocyte activation. *J Exp Med* **192**, 1027-1034 (2000).

8. Tseng, S.Y. *et al.* B7-DC, a new dendritic cell molecule with potent costimulatory properties for T cells. *J Exp Med* **193**, 839-846 (2001).

9. Latchman, Y. *et al.* PD-L2 is a second ligand for PD-1 and inhibits T cell activation. *Nat Immunol* **2**, 261-268 (2001).

10. Dong, H., Zhu, G., Tamada, K. & Chen, L. B7-H1, a third member of the B7 family, co-stimulates T-cell proliferation and interleukin-10 secretion. *Nat Med* **5**, 1365-1369 (1999).

11. Sheppard, K.A. *et al.* PD-1 inhibits T-cell receptor induced phosphorylation of the ZAP70/CD3zeta signalosome and downstream signaling to PKCtheta. *FEBS Lett* **574**, 37-41 (2004).

12. Hui, E. *et al.* T cell costimulatory receptor CD28 is a primary target for PD-1-mediated inhibition. *Science* **355**, 1428-1433 (2017).

13. Pitt, J.M. *et al.* Resistance Mechanisms to Immune-Checkpoint Blockade in Cancer: Tumor-Intrinsic and -Extrinsic Factors. *Immunity* **44**, 1255-1269 (2016).

14. Platten, M., Wick, W. & Van den Eynde, B.J. Tryptophan catabolism in cancer: beyond IDO and tryptophan depletion. *Cancer Res* **72**, 5435-5440 (2012).

15. Coussens, L.M., Zitvogel, L. & Palucka, A.K. Neutralizing tumor-promoting chronic inflammation: a magic bullet? *Science* **339**, 286-291 (2013).

16. Joyce, J.A. & Fearon, D.T. T cell exclusion, immune privilege, and the tumor microenvironment. *Science* **348**, 74-80 (2015).

17. Kim, K. *et al.* Eradication of metastatic mouse cancers resistant to immune checkpoint blockade by suppression of myeloid-derived cells. *Proc Natl Acad Sci U S A* **111**, 11774-11779 (2014).

18. Koyama, S. *et al.* Adaptive resistance to therapeutic PD-1 blockade is associated with upregulation of alternative immune checkpoints. *Nat Commun* **7**, 10501 (2016).

19. Chang, C.H. *et al.* Metabolic Competition in the Tumor Microenvironment Is a Driver of Cancer Progression. *Cell* **162**, 1229-1241 (2015).

20. Malmberg, K.J. *et al.* A short-term dietary supplementation of high doses of vitamin E increases T helper 1 cytokine production in patients with advanced colorectal cancer. *Clin Cancer Res* **8**, 1772-1778 (2002).

21. Hooper, L.V., Littman, D.R. & Macpherson, A.J. Interactions between the microbiota and the immune system. *Science* **336**, 1268-1273 (2012).

22. Vetizou, M. *et al.* Anticancer immunotherapy by CTLA-4 blockade relies on the gut microbiota. *Science* **350**, 1079-1084 (2015).

23. Routy, B. *et al.* Gut microbiome influences efficacy of PD-1-based immunotherapy against epithelial tumors. *Science* **359**, 91-97 (2018).

24. Sivan, A. *et al.* Commensal Bifidobacterium promotes antitumor immunity and facilitates anti-PD-L1 efficacy. *Science* **350**, 1084-1089 (2015).

25. Sharma, P., Hu-Lieskovan, S., Wargo, J.A. & Ribas, A. Primary, Adaptive, and Acquired Resistance to Cancer Immunotherapy. *Cell* **168**, 707-723 (2017).

26. Van Allen, E.M. *et al.* Genomic correlates of response to CTLA-4 blockade in metastatic melanoma. *Science* **350**, 207-211 (2015).

27. Sharma, P. & Allison, J.P. Immune checkpoint targeting in cancer therapy: toward combination strategies with curative potential. *Cell* **161**, 205-214 (2015).

28. Hodi, F.S. *et al.* Immunologic and clinical effects of antibody blockade of cytotoxic T lymphocyte-associated antigen 4 in previously vaccinated cancer patients. *Proc Natl Acad Sci U S A* **105**, 3005-3010 (2008).

29. Vanneman, M. & Dranoff, G. Combining immunotherapy and targeted therapies in cancer treatment. *Nat Rev Cancer* **12**, 237-251 (2012).

30. John, L.B., Kershaw, M.H. & Darcy, P.K. Blockade of PD-1 immunosuppression boosts CAR T-cell therapy. *Oncoimmunology* **2**, e26286 (2013).

31. Cherkassky, L. *et al.* Human CAR T cells with cell-intrinsic PD-1 checkpoint blockade resist tumor-mediated inhibition. *J Clin Invest* **126**, 3130-3144 (2016).

32. Blackburn, S.D. *et al.* Coregulation of CD8+ T cell exhaustion by multiple inhibitory receptors during chronic viral infection. *Nat Immunol* **10**, 29-37 (2009).

33. Johnston, R.J. *et al.* The immunoreceptor TIGIT regulates antitumor and antiviral CD8(+) T cell effector function. *Cancer Cell* **26**, 923-937 (2014).

34. Wolchok, J.D. *et al.* Nivolumab plus ipilimumab in advanced melanoma. *N Engl J Med* **369**, 122-133 (2013).

35. Callahan, M.K. *et al.* Nivolumab Plus Ipilimumab in Patients With Advanced Melanoma: Updated Survival, Response, and Safety Data in a Phase I Dose-Escalation Study. *J Clin Oncol* **36**, 391-398 (2018).

36. Goldberg, M.V. & Drake, C.G. LAG-3 in Cancer Immunotherapy. *Curr Top Microbiol Immunol* **344**, 269-278 (2011).

37. Woo, S.R. *et al.* Immune inhibitory molecules LAG-3 and PD-1 synergistically regulate T-cell function to promote tumoral immune escape. *Cancer Res* **72**, 917-927 (2012).

38. Sakuishi, K. *et al.* Targeting Tim-3 and PD-1 pathways to reverse T cell exhaustion and restore anti-tumor immunity. *J Exp Med* **207**, 2187-2194 (2010).

39. Vinay, D.S. & Kwon, B.S. 4-1BB (CD137), an inducible costimulatory receptor, as a specific target for cancer therapy. *BMB Rep* **47**, 122-129 (2014).

40. Kocak, E. *et al.* Combination therapy with anti-CTL antigen-4 and anti-4-1BB antibodies enhances cancer immunity and reduces autoimmunity. *Cancer Res* **66**, 7276-7284 (2006).

41. Mitsui, J. *et al.* Two distinct mechanisms of augmented antitumor activity by modulation of immunostimulatory/inhibitory signals. *Clin Cancer Res* **16**, 2781-2791 (2010).

42. Bretscher, P.A. A two-step, two-signal model for the primary activation of precursor helper T cells. *Proc Natl Acad Sci U S A* **96**, 185-190 (1999).

43. Sharpe, A.H. & Freeman, G.J. The B7-CD28 superfamily. *Nat Rev Immunol* **2**, 116-126 (2002).

44. Flajnik, M.F., Tlapakova, T., Criscitiello, M.F., Krylov, V. & Ohta, Y. Evolution of the B7 family: co-evolution of B7H6 and NKp30, identification of a new B7 family member, B7H7, and of B7's historical relationship with the MHC. *Immunogenetics* **64**, 571-590 (2012).

45. Zhao, R. *et al.* HHLA2 is a member of the B7 family and inhibits human CD4 and CD8 T-cell function. *Proc Natl Acad Sci U S A* **110**, 9879-9884 (2013).

46. McAdam, A.J., Schweitzer, A.N. & Sharpe, A.H. The role of B7 co-stimulation in activation and differentiation of CD4+ and CD8+ T cells. *Immunol Rev* **165**, 231-247 (1998).

47. Hathcock, K.S., Laszlo, G., Pucillo, C., Linsley, P. & Hodes, R.J. Comparative analysis of B7-1 and B7-2 costimulatory ligands: expression and function. *J Exp Med* **180**, 631-640 (1994).

48. Freeman, G.J. *et al.* Cloning of B7-2: a CTLA-4 counter-receptor that costimulates human T cell proliferation. *Science* **262**, 909-911 (1993).

49. Borriello, F. *et al.* B7-1 and B7-2 have overlapping, critical roles in immunoglobulin class switching and germinal center formation. *Immunity* **6**, 303-313 (1997).

50. Stamper, C.C. *et al.* Crystal structure of the B7-1/CTLA-4 complex that inhibits human immune responses. *Nature* **410**, 608-611 (2001).

51. Schwartz, J.C., Zhang, X., Fedorov, A.A., Nathenson, S.G. & Almo, S.C. Structural basis for co-stimulation by the human CTLA-4/B7-2 complex. *Nature* **410**, 604-608 (2001).

52. Rennert, P. *et al.* The IgV domain of human B7-2 (CD86) is sufficient to co-stimulate T lymphocytes and induce cytokine secretion. *Int Immunol* **9**, 805-813 (1997).

53. Suntharalingam, G. *et al.* Cytokine storm in a phase 1 trial of the anti-CD28 monoclonal antibody TGN1412. *N Engl J Med* **355**, 1018-1028 (2006).

54. Arlauckas, S.P. *et al.* In vivo imaging reveals a tumor-associated macrophage-mediated resistance pathway in anti-PD-1 therapy. *Sci Transl Med* **9** (2017).

55. Zhang, X., Schwartz, J.C., Almo, S.C. & Nathenson, S.G. Crystal structure of the receptor-binding domain of human B7-2: insights into organization and signaling. *Proc Natl Acad Sci U S A* **100**, 2586-2591 (2003).

56. Complete sequence and gene map of a human major histocompatibility complex. The MHC sequencing consortium. *Nature* **401**, 921-923 (1999).

57. Compte, E., Pontarotti, P., Collette, Y., Lopez, M. & Olive, D. Frontline: Characterization of BT3 molecules belonging to the B7 family expressed on immune cells. *Eur J Immunol* **34**, 2089-2099 (2004).

58. Afrache, H., Gouret, P., Ainouche, S., Pontarotti, P. & Olive, D. The butyrophilin (BTN) gene family: from milk fat to the regulation of the immune response. *Immunogenetics* **64**, 781-794 (2012).

59. Arnett, H.A. *et al.* BTNL2, a butyrophilin/B7-like molecule, is a negative costimulatory molecule modulated in intestinal inflammation. *J Immunol* **178**, 1523-1533 (2007).

60. Nguyen, T., Liu, X.K., Zhang, Y. & Dong, C. BTNL2, a butyrophilin-like molecule that functions to inhibit T cell activation. *J Immunol* **176**, 7354-7360 (2006).

61. Fuertes Marraco, S.A., Baumgaertner, P., Legat, A., Rufer, N. & Speiser, D.E. A stepwise protocol to coat aAPC beads prevents out-competition of anti-CD3 mAb and consequent experimental artefacts. *J Immunol Methods* **385**, 90-95 (2012).

62. Orozco, G. *et al.* Analysis of a functional BTNL2 polymorphism in type 1 diabetes, rheumatoid arthritis, and systemic lupus erythematosus. *Hum Immunol* **66**, 1235-1241 (2005).

63. Valentonyte, R. *et al.* Sarcoidosis is associated with a truncating splice site mutation in BTNL2. *Nat Genet* **37**, 357-364 (2005).

64. Zhu, B., Cai, G., Hall, E.O. & Freeman, G.J. In-fusion assembly: seamless engineering of multidomain fusion proteins, modular vectors, and mutations. *Biotechniques* **43**, 354-359 (2007).

65. Fischer, M. *et al.* Expression of CCL5/RANTES by Hodgkin and Reed-Sternberg cells and its possible role in the recruitment of mast cells into lymphomatous tissue. *Int J Cancer* **107**, 197-201 (2003).

66. Shi, Y. *et al.* Granulocyte-macrophage colony-stimulating factor (GM-CSF) and T-cell responses: what we do and don't know. *Cell Res* **16**, 126-133 (2006).

67. Hathcock, K.S. *et al.* Identification of an alternative CTLA-4 ligand costimulatory for T cell activation. *Science* **262**, 905-907 (1993).

68. Lisanti, M.P., Caras, I.W. & Rodriguez-Boulan, E. Fusion proteins containing a minimal GPI-attachment signal are apically expressed in transfected MDCK cells. *J Cell Sci* **99 (Pt 3)**, 637-640 (1991).

69. Marshall, R.D. The nature and metabolism of the carbohydrate-peptide linkages of glycoproteins. *Biochem Soc Symp*, 17-26 (1974).

70. Dvir, S. *et al.* Deciphering the rules by which 5'-UTR sequences affect protein expression in yeast. *Proc Natl Acad Sci U S A* **110**, E2792-2801 (2013).

71. Kober, L., Zehe, C. & Bode, J. Optimized signal peptides for the development of high expressing CHO cell lines. *Biotechnol Bioeng* **110**, 1164-1173 (2013).

72. Peach, R.J. *et al.* Both extracellular immunoglobin-like domains of CD80 contain residues critical for binding T cell surface receptors CTLA-4 and CD28. *J Biol Chem* **270**, 21181-21187 (1995).

73. Girard, T., Gaucher, D., El-Far, M., Breton, G. & Sekaly, R.P. CD80 and CD86 IgC domains are important for quaternary structure, receptor binding and co-signaling function. *Immunol Lett* **161**, 65-75 (2014).

74. Rouas, R. *et al.* Lentiviral-mediated gene delivery in human monocyte-derived dendritic cells: optimized design and procedures for highly efficient transduction compatible with clinical constraints. *Cancer Gene Ther* **9**, 715-724 (2002).

75. Chapoval, A.I. *et al.* B7-H3: a costimulatory molecule for T cell activation and IFN-gamma production. *Nat Immunol* **2**, 269-274 (2001).

76. Prasad, D.V. *et al.* Murine B7-H3 is a negative regulator of T cells. *J Immunol* **173**, 2500-2506 (2004).

77. Suh, W.K. *et al.* The B7 family member B7-H3 preferentially down-regulates T helper type 1-mediated immune responses. *Nat Immunol* **4**, 899-906 (2003).

78. Shrimali, R.K. *et al.* Concurrent PD-1 Blockade Negates the Effects of OX40 Agonist Antibody in Combination Immunotherapy through Inducing T-cell Apoptosis. *Cancer Immunol Res* **5**, 755-766 (2017).

79. Lundegaard, C., Lund, O. & Nielsen, M. Prediction of epitopes using neural network based methods. *J Immunol Methods* **374**, 26-34 (2011).